DTIC FILE COPY

AD-A224 189

Unclassified
SECURITY CLASSIFICATION OF THIS PAGE

88 - 0008

DTIC
ELECTE
JUL 17 1990
S D
D

1a. REPORT SECURITY CLASSIFICATION Unclassified	**1b. RESTRICTIVE MARKINGS**
2a. SECURITY CLASSIFICATION AUTHORITY	**3 DISTRIBUTION/AVAILABILITY OF REPORT** Statement A. per DTIC DISTRIBUTION STATEMENT A Approved for public release Distribution Unlimited
2b. DECLASSIFICATION / DOWNGRADING SCHEDULE	
4. PERFORMING ORGANIZATION REPORT NUMBER(S) 896988	**5. MONITORING ORGANIZATION REPORT NUMBER(S)**
6a. NAME OF PERFORMING ORGANIZATION Optical Sciences Center **6b. OFFICE SYMBOL** *(If applicable)*	**7a. NAME OF MONITORING ORGANIZATION** Rome Air Development Center
6c. ADDRESS *(City, State, and ZIP Code)* University of Arizona Tucson, Arizona	**7b ADDRESS** *(City, State, and ZIP Code)* Griffiss Air Force Base New York 13441
8a. NAME OF FUNDING / SPONSORING ORGANIZATION Rome Air Development Center **8b OFFICE SYMBOL** *(If applicable)*	**9 PROCUREMENT INSTRUMENT IDENTIFICATION NUMBER** F30602-83-K-0151
8c. ADDRESS *(City, State, and ZIP Code)* Griffiss Air Force Base New York 13441	**10 SOURCE OF FUNDING NUMBERS** PROGRAM ELEMENT NO / PROJECT NO / TASK NO / WORK UNIT ACCESSION

11 TITLE *(Include Security Classification)*
BRDF Scatter Research

12. PERSONAL AUTHOR(S)
William L. Wolfe

13a. TYPE OF REPORT	**13b. TIME COVERED**	**14. DATE OF REPORT** *(Year, Month, Day)*	**15 PAGE COUNT**
Final	FROM 8/1/83 TO 8/28/86	December 15, 1987	61

16. SUPPLEMENTARY NOTATION

17 COSATI CODES			**18 SUBJECT TERMS** *(Continue on reverse if necessary and identify by block number)*
FIELD	GROUP	SUB-GROUP	

19. ABSTRACT *(Continue on reverse if necessary and identify by block number)*

Portable scatterometers are briefly described. Applications of the vector electromagnetic theory are made to wavelength and angle scaling and used to show the limits of the different scatterometers. Appendices give design details and instructions for use.

DO NOT REMOVE
%DAAAAAA9200647V

20. DISTRIBUTION / AVAILABILITY OF ABSTRACT ☒ UNCLASSIFIED/UNLIMITED ☐ SAME AS RPT ☐ DTIC USERS	**21. ABSTRACT SECURITY CLASSIFICATION** Unclassified
22a. NAME OF RESPONSIBLE INDIVIDUAL Floyd L. Lance	**22b. TELEPHONE** *(Include Area Code)* 602-621-6996 **22c. OFFICE SYMBOL**

DD FORM 1473, 84 MAR 83 APR edition may be used until exhausted.
All other editions are obsolete.

SECURITY CLASSIFICATION OF THIS PAGE
Unclassified

90 07 16 423

Report F30602-83-K-0151

OPTICAL SCATTER RESEARCH

William L. Wolfe
Optical Sciences Center
University of Arizona
Tucson, Arizona 85721
(602) 621-3034

25 November 1987

A Final Report for the Period of August 1, 1983, to August 28, 1986.

Approved for public release; distribution unlimited

Prepared for:

AFSC
ROME AIR DEVELOPMENT CENTER
Griffiss Air Force Base, New York 13441

DISCLAIMER

TABLE OF CONTENTS

ABSTRACT

Comparisons of theory and experiment have shown that the vector electromagnetic theory of scattering from microrough surfaces is largely in agreement with measurements. Data were taken at several wavelengths, for several angles of incidence, and for several combinations of polarization. The agreement for the most part is within experimental error. Surface data were obtained on the samples by stylus profilometry and interferometric probes. The data were used to conceive and design an optical shop scatterometer, using a helium-neon laser and ten silicon detectors. The instrument was shown to be capable of measuring mirror samples of reasonable roughness, and scaling to other wavelengths could then be accomplished. Thus, a simple instrument could be used in the optical shop to characterize mirrors up to 2 m in diameter. Very good mirrors could not be scaled. The rollover point in the curves was too close to the specular direction; values of the surface roughness and correlation length could not be determined independently.

A second instrument, operating at about 10 μm, was designed and a laboratory model was constructed. A noise equivalent BRDF of $10^{-4}sr^{-1}$ at 2^0 from specular was demonstrated with an instrument that has 1-m-long arms. Thus, it was shown that a device consisting of a CO_2 laser and pyroelectric detectors can be constructed that is capable of characterizing mirrors of very good quality.

Appendices give design details and instructions for use.

INTRODUCTION

This is the final report on a study by the University of Arizona for the Rome Air Develoment Center at Griffiss Air Force Base. The study had as its primary goal the development of a scatterometer that could be used in an optical shop on finished mirrors with diameters as large as two meters. One of the measurement goals was a bidirectional reflectance distribution function (BRDF) of $10^{-3}sr^{-1}$ one degree from specular at 10.6 μm. The details of the work statement are given in Appendix A.

Theoretical developments were to be carried out to do the appropriate wavelength and angle scaling. They were to be accompanied by appropriate measurements.

PRINCIPAL RESULTS

Two versions of a scatterometer were constructed using a helium-neon laser, chopper, silicon detectors, and appropriate electronics. One version simply used ten detectors, properly spaced to obtain the scatter measurements. This instrument is described in a published paper that is reproduced as Appendix B. The instrument was demonstrated at RADC in 1986. Instructions for its use are given in Appendix C.

One shortcoming of that instrument was its limitation in obtaining angularly resolved data near the specular direction. Therefore, a second instrument was delivered and demonstrated in 1987. It used an array of silicon detectors in place of the single detector closest to the specular reflection direction. This instrument was described in another paper. A copy is attached as Appendix D. There was still a problem resulting from instrument background.

A third instrument was therefore designed. It was based on a CO_2 laser and ten pyroelectric detectors. The same geometry, a chopper, and appropriate electronics were designed. Because it was imperative that good performance near specular be achieved, we carried out laboratory experiments. We obtained a noise equivalent BRDF of $10^{-4}sr^{-1}$ at 2^0 from specular at 10.6 μm. A presently unpublished article describing this is enclosed as Appendix E.

TECHNICAL DISCUSSION

This section provides some of the results of the theory of scattering so that the instrument designs and limitations may be better understood.

Some Scaling Laws

Several authors have published theoretical results of scattering from surfaces with roughness less than the wavelength of the radiation.[1-15] The basic result is

$$\begin{aligned}
\rho_b &= \text{BRDF} \\
\rho_b &= F(\lambda)F(\theta)F(s) \\
F(\lambda) &= \text{wavelength factor} \\
F(\theta) &= \text{angle factor} \\
F(s) &= \text{surface factor} \\
\text{BRDF} &= \text{scattered radiance divided by incident irradiance.}
\end{aligned}$$

The BRDF may be written as the product of three factors: wavelength, geometry, and surface. The first of these is either $1/\lambda^3$ or $1/\lambda^4$ depending on the details of the model. The second is a function of the dielectric constant and angles of incidence and scatter. It is a relatively weak function, and it may be ignored in the ensuing analysis. The third factor relates directly to the surface. It is, in fact, the variance spectrum of the surface-height distribution. For a random surface with exponential autocorrelation, it can be shown to have one of two spectra:

$$\rho_b = \frac{k^3 F(\theta)\sigma^2 \ell}{1+p^2\ell^2} \text{ or } \frac{k^4 F(\theta)\sigma^2 \ell^2}{(1+p^2\ell^2)^{3/2}}$$

where

$$\begin{aligned}
k &= 2\pi/\lambda \\
\sigma &= \text{rms roughness} \\
\ell &= \text{correlation length} \\
p &= k(\beta-\beta_0) \\
&= k(\sin\theta-\sin\theta_0) \\
\theta &= \text{scatter angle} \\
\theta_0 &= \text{specular angle.}
\end{aligned}$$

The first relates to a one-dimensional transform; the second to a two-dimensional version. Most data fit the first form.

We are interested in how these scale with wavelength and angle. We ignore $F(\theta)$, that is, we let $F(\theta)$ be 1, and investigate the linear asymptotes of these expressions, for $p^2\ell^2 \ll 1$ and $p^2\ell^2 \gg 1$. In the first case

$$\rho_b = k^3\sigma^2\ell \text{ or } \rho_b = k^4\sigma^2\ell^2 \quad .$$

The BRDF is a straight, horizontal line. The two-dimensional version is $2\pi\ell/\lambda$ times the one-dimensional one. We shall see that this is often not significant. In the other region

$$\text{BRDF} = \frac{2k^3\sigma^2\ell}{\pi p^2\ell^2} = \frac{2\sigma^2}{\pi\lambda\ell(\beta-\beta_0)^2}$$

$$\text{BRDF} = \frac{2k^4\sigma^2\ell^2}{p^3\ell^3} = \frac{2\sigma^2}{\lambda\ell(\beta-\beta_0)^3} \quad .$$

Finally, the asymptotes for both forms intersect at $p = 1/\ell$. Several things arise from these theoretical results: the asymptotic curves are straight, horizontal lines at small angles and they are slopes of either -2 or -3 at larger angles when plotted logarithmically. The intersection is at $p = 1/\ell$.

Validity of Scaling Theories

Several theories were investigated, and appropriate data were taken to test these theories. This information has been published in the Journal of the Optical Society of America, and a reprint is included here as Appendix F. The results are, in essence, for specular surfaces, that the vector electromagnetic theory is valid; the scalar theory is not. For measurements in the plane of incidence, the one-dimensional transform applies; the two-dimensional version does not.

Appendix G is a reprint from an SPIE Proceedings that also discusses the inference of surface parameters by various techniques. The one we prefer is fitting the shape of the curve with both the correlation length and the rms roughness.

Measurements of Surface Parameters from BRDF Values

Two values can be inferred from the BRDF vs $\beta - \beta_0$ curves, like these, the rms roughness σ and the autocorrelation length ℓ. Thus we need at least two measurements. If we do it on the slope, we have

$$\rho_{b_1} = \frac{\sigma^2}{(\lambda\ell(\beta-\beta_0))_1^2}$$

$$\rho_{b_2} = \frac{\sigma^2}{(\lambda\ell(\beta-\beta_0))_2^2} \quad .$$

The subscripts 1 and 2 represent measurement values. We assume, as is the custom, that these were both measured at the same wavelength and that neither σ nor ℓ changed. Then we have the simple relationship

$$\frac{\rho_{b_1}}{\rho_{b_2}} = \frac{(\beta-\beta_0)_2^2}{(\beta-\beta_0)_1^2} \quad .$$

They are linearly related. This means that to infer ℓ, and therefore σ, we must at least approach the region where $p = 1/\ell$. A typical correlation length for a good surface is 10 μm. Then at 0.6328 μm,

$$\beta-\beta_0 = \lambda/2\pi\ell = 0.01 \quad .$$

If we also use an rms roughness of 10 nm (0.01 μm), we can find the BRDF at this spatial frequency:

$$\begin{aligned} \text{BRDF} &= k^3\sigma^2\ell/\lambda \\ &= \left[\frac{2\pi}{0.6328}\right]^3(0.01)^2 10/2 \\ &\cong 0.49\ \text{sr}^{-1} \quad . \end{aligned}$$

This is a difficult measurement to achieve. The specification of 10^{-3}sr^{-1} at 1° means that the product of the rms roughness and the correlation length must be about 10^{-6} μm^3. This is equivalent to a mirror with a 1-nm roughness and a 1-μm correlation length, or a 0.3-nm roughness and 10-μm correlation length, very good mirrors indeed. In fact, on some of the better mirrors the intersection could not be determined.

The intersection point is wavelength dependent. In fact, it is linearly dependent upon the wavelength. Thus, in moving from 0.63 μm to 10.6 μm, the β - β_0 value of the intersection should move from 0.01 to about 0.17. However, the flatband BRDF will be reduced by a factor of almost five thousand. The measurement is better made at 10 μm, which is why we developed the infrared instrument. The infrared instrument, as is shown in Appendix E, would measure a BRDF of 10^{-3}sr^{-1} with about 10% error as close to specular as 2° (β - β_0 = 0.035). Lower BRDF values would be possible at larger angles. The noise equivalent BRDF of about 6×10^{-6} sr^{-1} would be obtained at about 6° (β - β_0 = 0.1). This is well below the indicated rolloff values. For instance, a sample with a correlation length of 10 μm and an rms roughness of 1 nm has roll-off values of β - β_0 = 0.16 and a corresponding BRDF value of 1.6×10^{-4} sr^{-1}. Unfortunately, there were insufficient funds for the construction of a final infrared unit; we were only able to show feasibility.

Non-Random Surfaces

The vector version of the electromagnetic theory in its basic form, which we have demonstrated to be the most accurate representation of smooth surfaces, requires the spectrum of the surface-height distribution. Diamond-turned samples do not have randomly polished surfaces. They may be characterized by the very fine grooves of the diamond tool as it advances. They are, in fact, weak gratings with a spatial frequency of $p = k(\beta - \beta_0)$. Thus (radian) spatial frequency is related to the spatial period s.

$$p = k(\beta - \beta_0) = 2\pi/s \quad .$$

Then

$$s = \lambda/(\beta-\beta_0)$$

$$\beta-\beta_0 = \lambda/s$$

for the equivalent correlation length. Thus, for example, for a wavelength of 0.63 μm and screw advance of 1 μm, there will be a peak at $\beta - \beta_0 = 0.6$. This is well into the region of effective measurement. For the peak to be at less than 0.1, the advance would have to be more than 6.3 μm. Some of our BRDF data have been used to calculate this screw advance with good agreement.

CONCLUSIONS

The vector electromagnetic theory is a good model for microrough surfaces. It incorporates three factors, the most important of which is the surface-height variance spectrum. It applies to both random and to diamond-turned surfaces in the plane of incidence. An instrument has been designed and constructed that can measure the BRDF of large samples at various points at a wavelength of 0.6328 μm. It can measure a BRDF of approximately 10^{-3} sr^{-1} as close as about $\beta - \beta_0 = 0.01$. Thus, it should be good for samples that have a correlation length of about 10 μm and an rms roughness of about 0.4 nm. Samples better than this can be measured but not scaled. An infrared scatterometer is feasible. A laboratory demonstration, using the geometry and components that would be incorporated in a final model, showed that a noise-equivalent BRDF of 10^{-4} sr^{-1} was obtained at an angle of 2^0 from the specular.

BIBLIOGRAPHY OF VECTOR SCATTERING THEORY

1. Elson, J. M., "Light scattering from semi-infinite media for non-normal incidence," Phys. Rev. B **12**, 2541 (1975).

2. Church, E. L., H. A. Jenkinson, and J. M. Zavada, "Measurement of the finish of diamond-turned metal surfaces by differential light scattering," Opt. Eng. **16**, 360 (1977).

3. Elson, J. M. and R. H. Ritchie, "Diffuse scattering and surface-plasmon generation by photons at a rough dielectric surface," Physicus Status Solidi **62**, 461 (1974).

4. Maradudin, A. A. and W. Zierau, "Effects of surface roughness on the surface-polariton dispersion relation," Phys. Rev. B **14**, 484 (1976).

5. Maradudin, A. A. and D. L. Mills, "Scattering and absorption of electromagnetic radiation by a semi-infinite medium in the presence of surface roughness," Phys. Rev. B **11**, 11392 (1975).

6. Kröger, E. and E. Kretschmann, "Scattering by slightly rough surfaces or thin films including plasma resonance emission," Zeitschrift für Physik, 237, 1 (1970).

7. Hill, N. R., "Integral-equation perturbative approach to optical scattering from rough surfaces," Phys. Rev. B **24**, 7112 (1981).

8. Marvin, A., F. Toigo, and V. Celli, "Light scattering from rough surfaces: General incidence angle and polarization," Phys. Rev. B **11**, 2777 (1975).

9. Church, E. L., H. A. Jenkinson, and J. M. Zavada, "Relationship between surface scattering and microtopographic features," Opt. Eng. **18**, 125 (1979).

10. Church, E. L. and J. M. Zavad, "Residual roughness of diamond turned optics," Appl. Opt. **14**, 1788 (1975).

11. Rice, S. O., "Reflection of electromagnetic waves from slightly rough surfaces," Communications in Pure and Applied Mathematics **4**, 351 (1951).

12. Bennett, M. E. and J. O. Porteus, "Relation between surface roughness and specular reflectance at normal incidence," J. Opt. Soc. Am. **51**, 123 (1961).

13. Elson, J. M. and H. E. Bennett, "Relation between the angular dependence of scattering and the statistical properties of optical surfaces," J. Opt. Soc. Am. **69**, 31 (1979).

14. Crowell, J. and R. H. Ritchie, "Surface-plasmon effect in the reflectance of a metal," J. Opt. Soc. Am. **60**, 794 (1970).

15. Toigo, F., A. Marvin, V. Celli, and N. R. Hill, "Optical properties of rough surfaces: General theory and the small roughness limit," Phys. Rev. B **15**, 5618 (1977).

APPENDIX A

STATEMENT OF WORK

The University of Arizona, in the development of the bidirectional reflectance distribution function (BRDF) scatterometer, shall accomplish the following tasks:

a. Compare established scatter theories to be able to predict a BRDF of 10^{-3} sr^{-1} at 1^0 from specular at 10.6 μm. The modeling of these theories shall be such that both the wavelength scaling to 10.6 μm and angular scaling to 1^0 are achievable.

b. Adapt the Arizona Scatterometer (AZSCAT) to measure steeply sloped and high-order aspheric ssurfaces at a minimum BRDF of $10^{-3}sr^{-1}$ at 1^0 from specular at 10.6 μm.

c. Measure appropriate specimens to adequately verify modeling of the scatter theory and to assess the adaptation of AZSCAT to the parameters specified in paragraph b above.

d. Design, fabricate, test and deliver a protable scatterometer that is capable of measuring or using appropriately scaled data to infer BRDF of $10^{-3}sr^{-1}$ or less at 1^0 from specular at 10.6 μm. The instrument shall be capable of measuring BRDF on a surface with F/1 or less and a high-order aspheric.

e. Verify the utility of the instrument to the design parameters using samples supplied by the Contractor and, if desired by the Government, those samples directed by the Contracting Officer.

f. Provide familiarization to a maximum of ten Government selected personnel in the application of data and the instrument to analyze the stray light properties of developmental or operational systems, at no more than three instructional sessions.

APPENDIX B

A Portable Scatterometer for Optical Shop Use

William L. Wolfe, Kathleen Magee and Douglas W. Wolfe

Optical Sciences Center, University of Arizona
Tucson, Arizona

Introduction

The scattering of optical components has become a more and more critical issue in modern sensor systems. This is a result of improved performance capabilities on the part of detectors and of optical elements themselves, as well as an increased awareness of the effects of scatter on system performance. There are several programs that evaluate scatter in complicated optical trains, the best known of which are APART and GUERAP (Arizona Paraxial Analysis of Radiative Transfer and General Unwanted Energy Radiation Analysis Program). These programs require component scatter data as inputs for the analysis and even the beginning design approaches. These data have generally been generated with laboratory instruments that were essentially goniometric radiometers. The data have been difficult to obtain and usually obtained for small representative samples of the real surfaces. If, in the process of manufacture of the parts a measurement of the scatter was made, it was done with a relatively crude jerry-rigged apparatus. Sometimes the measurements made this way were quite accurate, but they were never easy.

This paper describes the design, construction and performance of a portable apparatus that can make scattering measurements on samples as large as 2 meters in diameter at 0.6328um for a 45-degree angle of incidence and a reasonably large range of scatter angles.

Theoretical background

The scattering of mirror surfaces is usually described in terms of the Bidirectional Reflectance Distribution Function (BRDF). Transmissive samples may be characterized by their values of Bidirectional Transmission Distribution Function (BTDF) and the general function can be the BSDF, where the S is for scattering. The instrumentation to be described here is a BRDF measurement device, meant for mirror samples, although it can be used equally well for diffuse reflectors. In its present configuration it cannot be used for the measurement of transparent-sample BTDF values.

Most of the data obtained on the BRDF values of both specular and diffuse samples have been presented in a log-log format in which the BRDF is plotted as a function of the surface spatial frequency for a fixed wavelength. The coordinate is commonly referred to as "beta-beta naught" or "delta beta." An example is shown in Fig. 1; it is the BRDF of a mirror measured at 10.6um. The values range from almost one to about one-millionth in units or reciprocal steradians. This of course is the reason for the logarithmic ordinate. The abscissa ranges from 0.01 to 2. The maximum possible value for the abscissa is 2, while the minimum theoretical value is zero. The minimum practical value for such measurements is about 0.018 or about one degree. Again, the range is more than an order of magnitude, and the small values are just as important (or more important) than the large ones.

A diffuse sample will, of course, require the same range for the independent value, but have a much smaller range of BRDF values. An example of a good, diffuse black is shown in Figure 2. Nothing is lost by presenting this information on a logarithmic scale.

Vector electromagnetic theory has been used to model the scattering from surfaces like these, which have roughness values much less than the wavelength of the incident light. The theory predicts that the BRDF can be written as the product of three factors, a wavelength factor, a geometry factor and a suface factor:

$$GBRDF=KGW$$

For measurements in the plane of incidence the wavelength factor is K cubed, where k is 2 pi divided by the wavelength. The geometry factor is a function of polarization; it is a smooth function of delta beta at least until the extremes of the measurement for ss and pp polarizations, and it is zero for the crossed polarizations in the plane of incidence. These factors are plotted in Fig. 3. The unpolarized version is the average of these two. The point is that these are smooth functions. The surface factor W is the power spectrum of the surface height distribution. For most mirrors made in the classical way this is a simple Lorentian that can be characterized by two asymptotes, one that is a horizontal straight line, and one that is a straight line with a slope of minus two. Surfaces that have been formed by diamond turning have superimposed on these curves a set of peaks that correspond to the advance of the tool.

The values for scattering out of the plane of incidence have not yet been modeled.

Instrumental overview

Consideration of the data presented in these figures indicate that the BRDF data can be obtained by illuminating the samples with laser light of the proper wavelength and measuring with an array of detectors; it should not be necessary to have a continuous distribution of them. Data for other angles of incidence and other wavelengths can be obtained by the scaling laws generated and developed from the theory. These are the basic concepts of the instrument design. The questions which arise are the placement of the detectors and the source with respect to the sample, the signal to noise ratios, the size of the illuminating spot, calibration, orientation, data taking and presentation of the results. We have not tried to design a research instrument, but rather one that can determine the properties of most mirrors and diffusers at most wavelengths for a reasonable range of scatter angles.

The instrument consists of a helium-neon laser, a chopper, a folding flat mirror, four silicon detectors with apertures, six with lenses, and amplifiers. The outputs of the amplifiers are sampled with a microcomputer and displayed on its screen. Options for printing the output are therby provided.

Geometry

The data should be taken at equal logarithmic increments from a value of 0.01 to 1. The values out to 2 are not really needed, and values below 0.01 are impossible to obtain. Values near 0.01 are indeed difficult. It appears that ten data points across this range are adequate because of the smoothness of most of the samples. Table 1 shows the detector placement for these, including a detector placed at the specular position.

But what angle of incidence should be used? If the sample is illuminated normally, then the specular direction cannot be measured. If the angle of incidence is too large, then the spot on the sample is too large, although this is not a serious constraint; the laser spot is collimated into a 14mm beam. The incidence angle is really dictated by the practical issues of how large the scatterometer can be and how far it must be from the test piece. These considerations must be traded off with the available range of delta beta for different angles of incidence. Either forward scatter or backscatter or some of each may be used. If the minimum practical incidence angle of 20 degrees is used then the range is 0 to 0.66. This is not as large as we would like. The range is smaller for 70 degrees, and the range for 10 degrees is still only 0 to 0.83. Backscattering seems more appropriate. The range then is from 0 to -(1+sinA). For 20 degrees this is 0 to -1.34; for 10,-1.17; for 30,-1.5; for 45,-1.71. Any angle of incidence gives a wide range of delta beta.

Practical geometries

The system should be relatively easy to use in the optical shop for mirrors up to about 2 meters in diameter. We have taken about 60 centimeters as the required height clearance for the system. We have chosen to mount all the components on an aluminium optical rail in the shape of a tee. This structure is supported by three commercial tripods. The leg of the tee is almost 2 meters long, while the crossbar is about 1.2 meters. This leaves, allowing for some clearances, about 130cm for the distance between the input beam and the specular return. For the clearance we have chosen and the length we used, the angle of incidence must be just about 45 degrees. We set it at that value, and then we readjusted the assumptions a little.

Signal to noise considerations

The noise equivalent BRDF is given by the following equation:

$$NEBRDF = \frac{SQR(AB)}{D^*}/OPcosA$$

where $SQR(A) = 0.1$ cm
$B = 1$ Hz
$D^* = 1E11$
$P = 1$ mW
$cosA = 1$
$O = 1E-4$ sr

Thus,

$$NEBRDF = 3E-5$$

The geometry chosen for the system results in a distance from the detector to the spot of about 85cm for the specular direction, and this means that to obtain a solid angle O of 1E-4 the collecting area must be 0.85 cm. This would be to obtain the NEBRFD specified. At that small angular distance from the specular direction, however, such sensitivity is not necessary. It is necessary at the other extreme, at the maximum backscatter angle. Thus, for the first four detectors, we have used only apertures, but for the next six we have used lenses to collect the radiation to obtain the sensitivity specified.

System details

A schematic diagram of the system is shown in Fig. 4 . A photograph is shown in Fig. 5 . The laser shown on top is a Hughes Series 3000 1mW helium-neon laser that has its output at 0.6328um. This shines on the folding flat mirror to the right of it through a synchronous chopper. The chopper is a Bentham 218 Variable Frequency Optical Chopper. The beam has a divergence of 1.3mr so that at the sample shown below, the spot has spread by 1.3mm, and is therefore 14mm in diameter. The folding flat is of our own manufacture. The specular beam enters the cylindrical tube shown where there are two crosshairs that constitute an aiming device. This device allows the orientation of the laser and the detectors to the local surface normal. It establishes the angular coordinate system to the extent that all the detectors are now in the plane of incidence and they are at the intended angular positions. The sight was the brainchild of A. G. DeBell and manufactured by us. We note in passing that this is not used as is a normal rifle sight. Rather, the user looks into the sight first from the front and then from the rear, each time at an angle to the optical axis. By trial and error he insures that the laser beam is centered on both crosshairs. This way he accomplishes the alignment without losing the use of his sighting eye.

The ten silicon detectors are all model UDT-455 Photops detectors. They come complete with integral preamplifiers. They were mounted in structures designed and built by us that can be adjusted to view the spot directly. This requires primarily one degree of freedom. There is some alignment allowed in the out-of-plane direction so that we can be sure they are in the plane. Figure 6 shows this arrangement.

Figure 7 is a schematic of the preamplifier that is integral with the Photops detector. These detector outputs are sampled with a combination of hardware and software. The hardware consists of several CMOS chips: 2-IH5108's, 2-74HC244's, 1-74HC373, 1-74HC74, 1-74HC138, 1-PGA200, 1-ICL7109 and miscellaneous components. The master controller is a Radio Shack TRS-80 Model 100 used for its properties as a terminal. The computer serves as the lockin amplifier, using the reference signal from the chopper.

Initial checkout

We started by simply checking the outputs against two samples for two different detectors. We used Macor as a representative of a highly reflective diffuse standard, and we used a mirror available in the lab as a prototype specular sample. Early tests showed that detector #1 which has a lens and is located about 80 degrees from specular gave about 1V signal from the Macor, while the mirror gave about 2mV signal; the noise was about 0.1mV rms and showed up on the oscilloscope as being white noise. A detector which has no lens and is about 15 degrees from specular gave respectively 20mV and 5mV. We can draw some conclusions from these data. The noise level is comparable to a BRDF of about 1E-4 for a detector with a lens and 1E-2 without. Some tuning should improve these values.

Calibration technique

The system needs careful handling by way of calibration. Two steps in general will be taken. The first is to use a diffuse isotropic sample like Macor. It will be measured by our laboratory scatterometer. Then the channel gains will be set in the software to provide the same BRDF profile. In this sense then the instrument is calibrated with Macor, or Halon or equivalent as a reference. Then a mirror sample will be used in the same way, first on the laboratory instrument and then with the portable scatterometer. The measurements should agree. Future use will be predicated on recalibration against the isotropic, diffuse standard.

Plans for the future

The system still does not do all that we would like it to do. It is mainly limited in its capability for making measurements close to the specular direction. One solution to this problem is the use of an array of silicon detectors instead of a single first detector. Of course this requires careful consideration and calibration of the beam profile in the area of the specular direction. A second area of investigation is the design and construction of a similar model in the 10um region of the spectrum. We are also addressing this question.

Acknowledgements

We would like to acknowledge the support of the U.S. Air Force and the advice and encouragement of Lt. Michael Rau; the mechanical design supervision of Langford Brod; and the constructional talents of Daniel Graham.

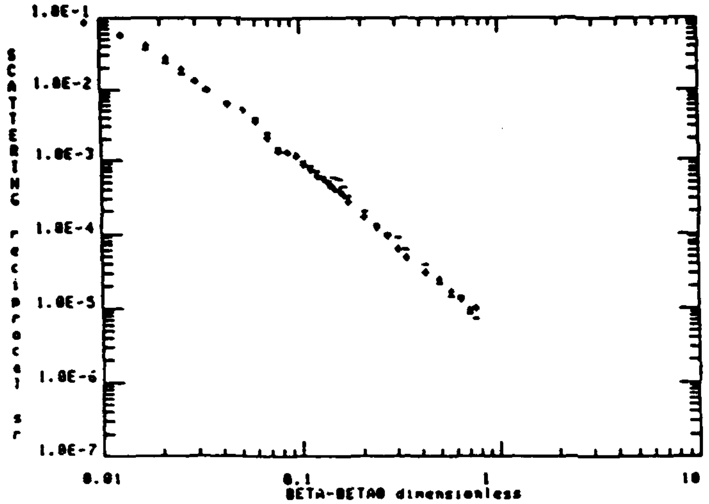

Fig. 1 BRDF of a Mirror at 10.6um

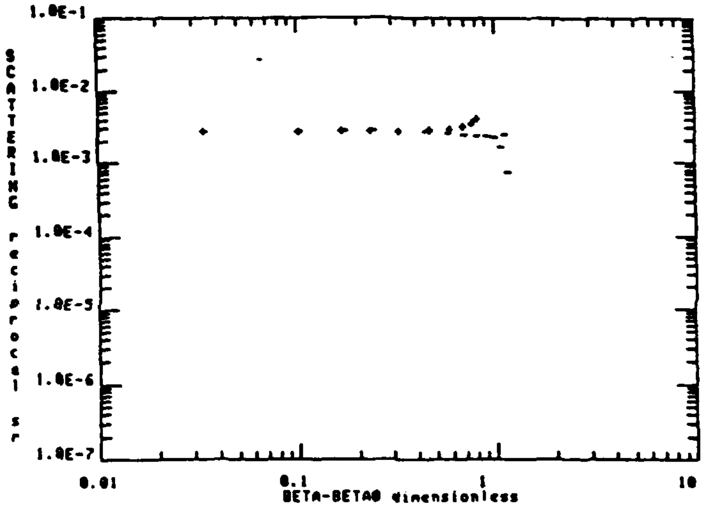

Fig. 2 BRDF of a Diffuse Black

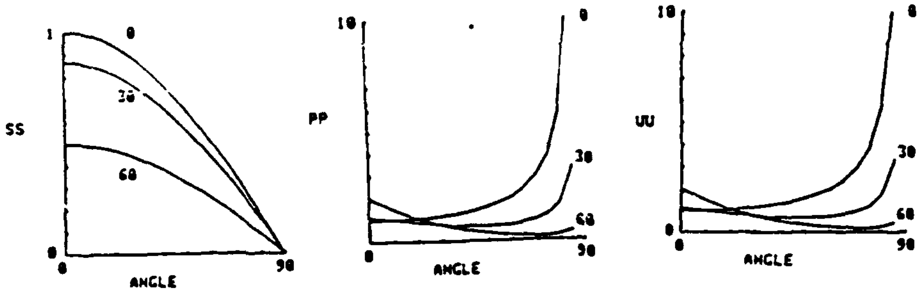

Figure 3. Geometric factors for ss, pp polarizations and unpolarized light.

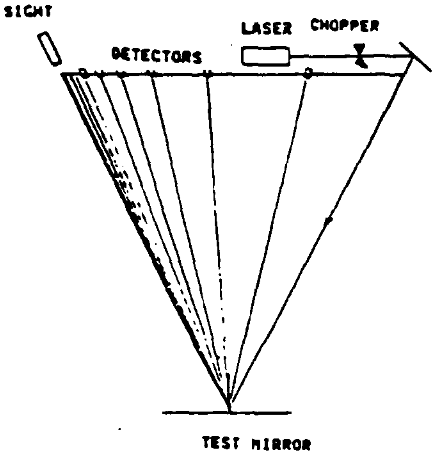

Figure 4. System Schematic diagram.

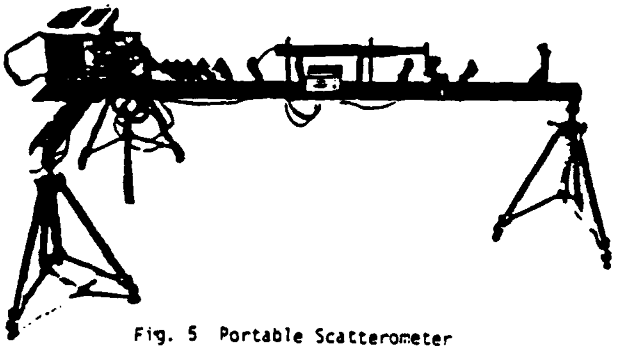

Fig. 5 Portable Scatterometer

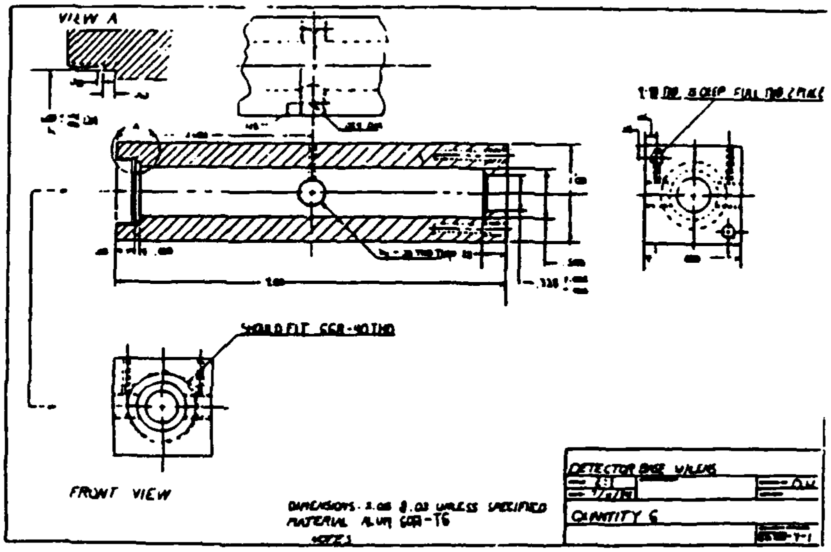

Fig. 6 Detector Base With Lens

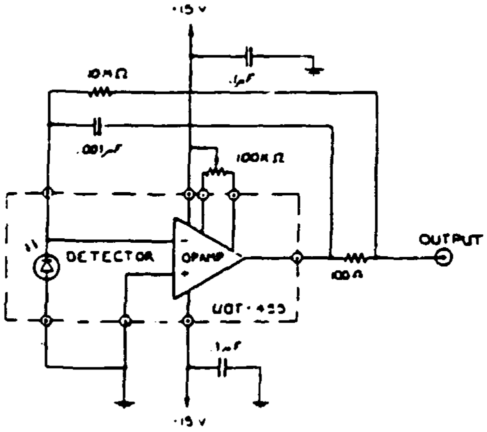

Fig. 7 Detector/Amplifier Schematic

Table 1. Detector Placement.

Dectector #	[illegible]	θ_s	L (m)	ΔL mm
1	0.000	20.00	.3640	0
2	0.017	18.97	.3437	3
3	0.028	18.30	.3307	13
4	0.047	17.16	.3088	
5	0.078	15.31	.2704	
6	0.130	12.24	.2169	
7	0.217	7.18	.1260	
8	0.362	-1.14	-.0199	
9	0.604	-15.16	-.2709	
10	1.009	-41.15	-.8739	

APPENDIX C

Calibration and Operation of the Portable Scatterometer

ASSEMBLY

1. Attach the crossrail to the optics rail with the gusset plate and install the two brackets under the gusset plate on each side of the optics rail (Fig. 1).

2. Attach the three swivel mounts to the corners of the optics rail and crossrail (Fig. 2). The legs of the tripods should be retracted, in their minimum extension position. Attach the tripods to the swivel mounts by inserting the threaded stud at the top of the tripod into a matching thread on the bottom of the swivel mount and turning the black knurled thumb wheel until the stud is firmly secured in the threaded hole.

3. The power to the main electronics cabinet should be off during assembly. Plug the laser and chopper power supplies into the 115 VAC outlets on the front panel on the main electronics cabinet. Connect the detector power cables and signal cables to the front panel also (Fig. 3); each cable is tagged with the appropriate detector number. The array power and signal cables should be plugged into the tenth set of sockets.

4. Connect the interface cable coming from the bottom of the TRS-80 model 100 computer to the interface connector on the rear panel of the main electronics cabinet.

CAUTION: When the interface cable is plugged into the main electronics cabinet, care must be taken to ensure that computer is never powered while the main electronics cabinet is not. FAILURE TO DO SO MAY RESULT IN LOSS OF ALL PROGRAMS AND DATA STORED IN RAM. Therefore, when the interface cable is plugged in, the 6 VDC power supply for the computer must be plugged into the 115 VAC time-delayed outlet indicated in Fig. 3. Note that whenever the main electronics cabinet power is turned off, though, the computer power must be reset. To reset it, turn the computer power switch located on the right side of the computer off and then on again. Once reset the computer will be powered whenever the main electronics cabinet is turned on again.

5. Connect one end of the chopper reference cable to the reference output connector on the chopper power supply and the other to the chopper reference connector on the front panel of the main electronics cabinet. Connect the chopping head cable to the chopper power supply also. The frequency dial of the chopper power supply should be set at about 28 for a 5 Hz chopper frequency.

6. If necessary, loosen the laser mount screws (Fig. 4) and remove any packing material. Position the laser so that it is approximately centered over the two mounts. The laser rotational position should be set so that the power cord is emerging from the laser body at the bottom. Re-tighten the laser mount screws.

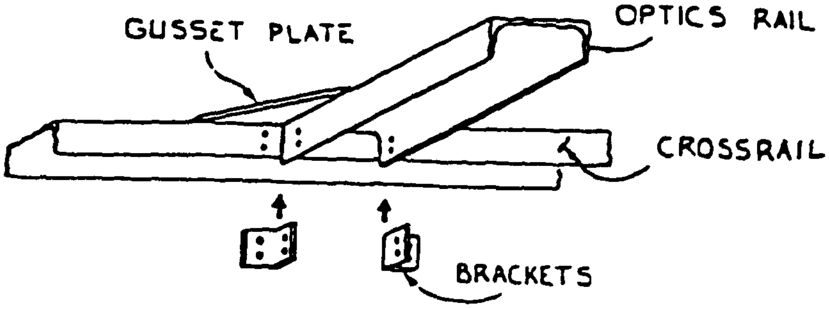

Figure 1.

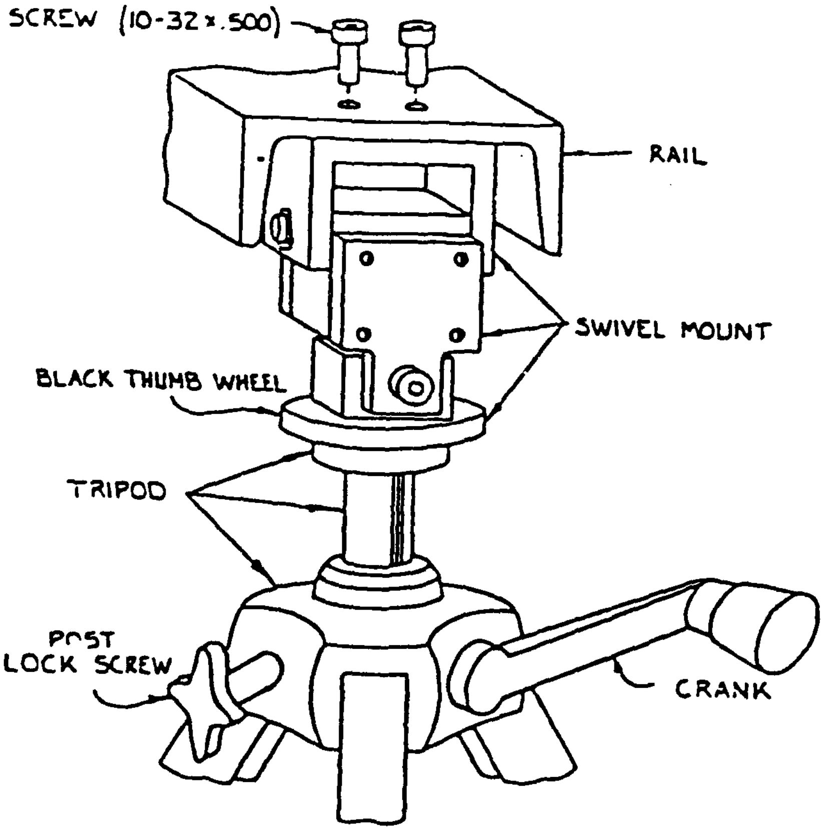

Figure 2.

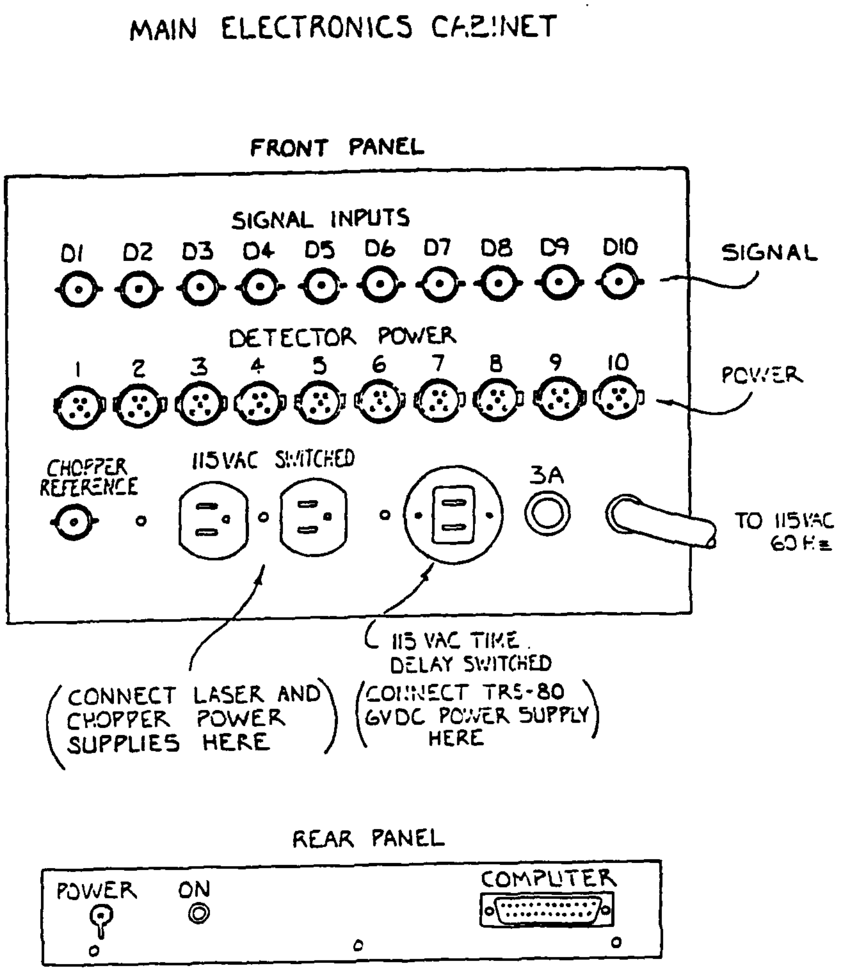

Figure 3.

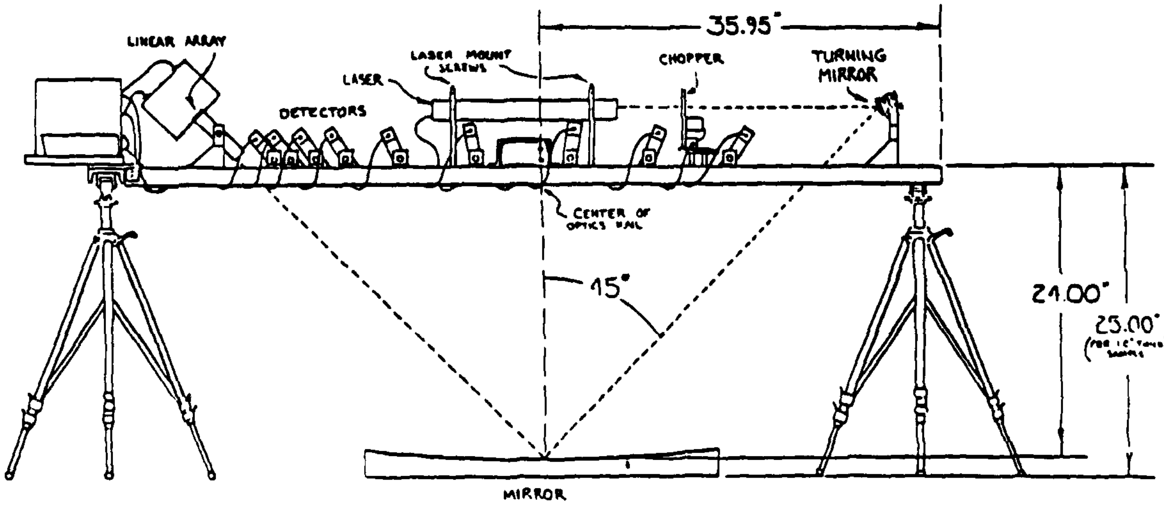

Figure 4.

OPERATION

Alignment

The instrument has been designed to measure the Bidirectional Reflectance Distribution Function (BRDF) for an incidence angle of 45 degrees (Fig. 4). The position of the laser, turning mirror, and linear array have been adjusted so that when the specular beam hits the center of a removable cross hair placed in the slit at the front of the array sighting tube and the center of the end array element at the same time, the angle of incidence is 45 degrees and all detectors are in the plane of incidence. During shipping and handling of the instrument the position of these items may have shifted slightly. The alignment can be checked as described below and if found to be out of alignment perform the calibration of the optical system described in the last section before making BRDF measurements.

1. Loosen the tripod post lock screws at the top of each tripod (Fig. 2) and crank up each tripod post until the top of the optics rail and crossrail is about 25 inches above the floor at each tripod. Temporarily tighten all tripod post lock screws.

2. The calibration of the optical system is based on the center being defined at 35.95 inches from the end of the optics rail (Fig. 5). Readjust the tripods until the top of the optics rail at the center is 25 inches above the floor on both sides (points A and B in Fig. 5) and the optics rail is approximately level. Due to a slight twist in the rail the ends may be slightly higher than the center. A circular level can be used to get the rail approximately level across the long dimension and level across the short dimension everywhere but near the crossrail (Fig. 5); tripod 2 may be need to be slightly higher than the other two. After adjustment all tripod post lock screws should be tight.

3. Turn on the laser power by flipping the power switch on the rear panel of the main electronics cabinet (up position). The chopper power supply can be turned off at this time. The axis of the laser beam should be parallel to the optics rail (Fig. 5). This alignment can be checked by setting a 12-inch machinist square upright on the optics rail near the laser output as shown in Fig.6; the edge of the scale should be two inches from the side of the optics rail. A piece of white paper placed in front of the scale edge can be used to determine whether or not the scale edge bisects the laser spot. Using the above procedure check the alignment of the laser beam near the turning mirror also. The axis of the laser beam should be two inches from the side of the optics rail near both the laser output and the turning mirror.

4. Place the pentaprism and prism housing under the optics rail on the floor so that the incident beam is approximately centered on the 1/2 inch diameter hole in the metal cover plate of the housing and the exit beam is reflected upward toward the array. Remove the beveled nylon cross hair at the front of the array sighting tube if necessary. Center the beam spot on the end array element by adjusting the pentaprism position and tilt as described below until the maximum signal amplitude is observed.

The signal can be measured by connecting the array signal cable to a voltmeter or an oscilloscope, and setting the switch on the array housing to "S" (select "S" for specular samples and "D" for diffuse samples). The chopper and computer power should be on at this time. When the computer is first turned on a directory of files is displayed with the cursor over BASIC. Hit ENTER and type the following sequence:

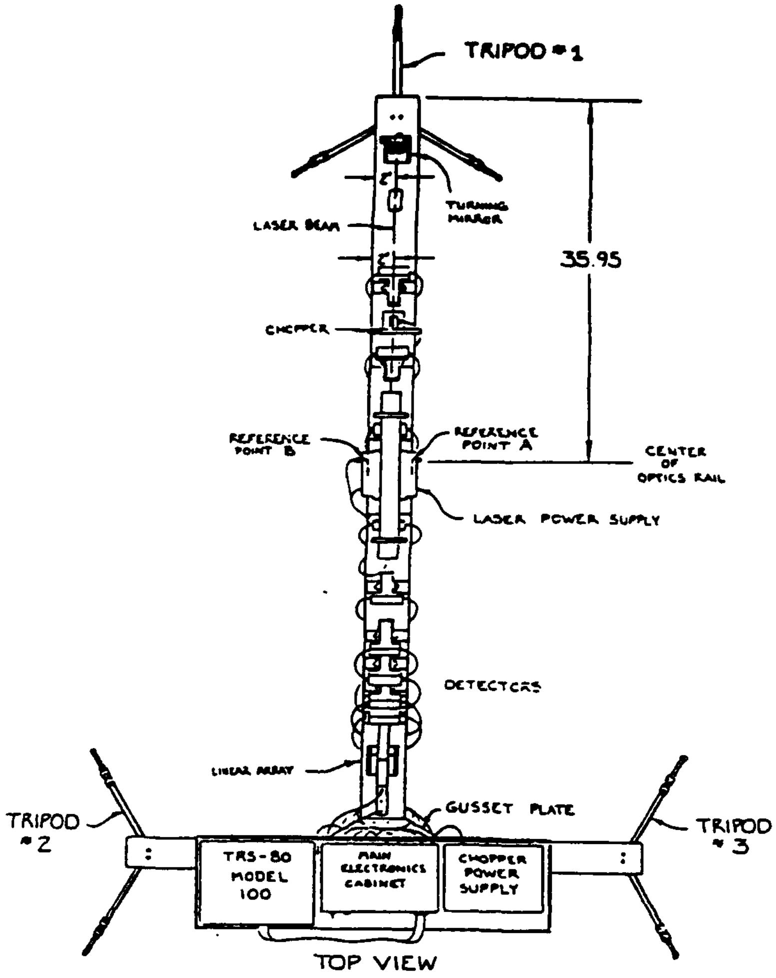

Figure 5.

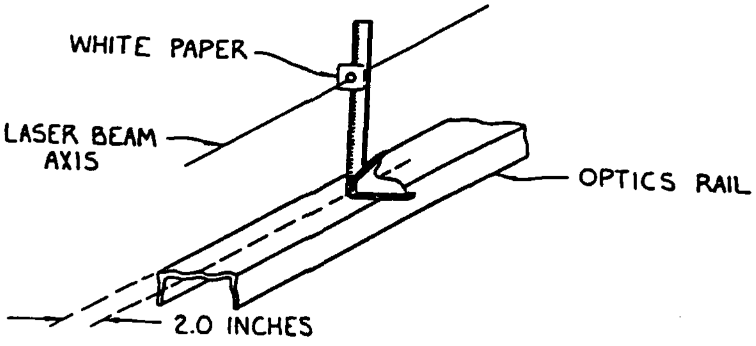

Figure 6.

```
OUT 119,0 <ENTER>
OUT 118,75 <ENTER>
```

The first line sets the gain of the programmable-gain-amplifier to one. The second line selects which array element preamp is switched to the signal cable; in this case the end array element is selected.

Misalignment of the beam spot on the vertical axis of the end array element is caused by an incorrect position of the prism along an axis common to the plane of incidence and the base of the prism (axis 1 of Fig. 7). Translate the prism along this axis until the maximum signal amplitude is observed. Note that the pentaprism produces an exit beam that is always 90 degrees from the incident beam regardless of the tilt of the prism about an axis perpendicular to the plane of incidence (axis 2 of Fig. 7), so no adjustment of the prism about this axis is necessary.

The plane of incidence, however, is dependent upon the tilt of the prism about axis 1 of Fig. 7. Any tilt of the prism about this axis will cause horizontal misalignment of the beam on the end array element. Adjust the fine pitch screw on the prism housing until the maximum signal amplitude is obtained.

The pentaprism may also be rotated about an axis perpendicular to the base (axis 3 of Fig 7). If the prism is rotated slightly about this axis, the exit beam will be parallel to the incident beam but translated sideways (Fig. 8). To avoid this the pentaprism should be rotated about axis 3 so that the beam incident on the prism and the beam reflected back toward the turning mirror by the prism are aligned in the same vertical plane (Fig. 9).

When the pentaprism is adjusted so that the maximum signal amplitude from the end array element is observed and the incident, exit, and reflected beams are in the same vertical plane, check the signal from the next array element from specular to be sure it is smaller then the signal at the end element. To do this type:

```
OUT 118,74 <ENTER>
```

which switches the next array element to the array signal cable. When the switch on the array housing is set on "S" the preamp gain is a factor of ten greater for this array element than for the end element, so take this into account when comparing the two signals. Reconnect the array signal cable to the front panel of the main electronics cabinet.

5. Install the beveled nylon cross hair on the pins next to the slit at the front of the array sighting tube so that the beveled surface faces outward and the cross hair covers the slit near the bottom end. If the instrument is correctly aligned the beam spot will be centered on the cross hairs.

6. Detector voltage data from the Macor sample collected by running the BRDF program stored in the TRS-80 model 100 computer can be used to determine whether or not the detectors need realignment. Replace the pentaprism with the rectangular Macor sample and mask assembly so that the beam spot is approximately centered on the Macor and run the BRDF program as directed in the next section, "Running the BRDF Program."

7. The detector voltages read by the computer with the Macor sample should be within 10% of those listed in Table 1.

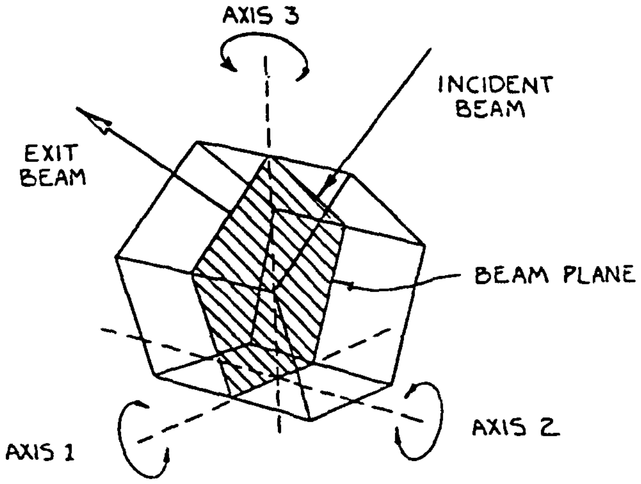

Figure 7.

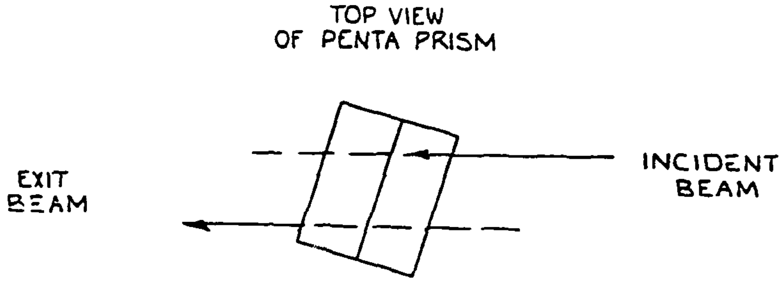

Figure 8.

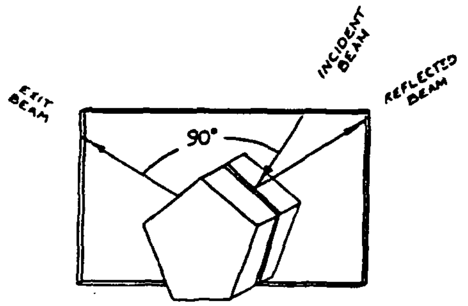

Figure 9.

Table 1.

Detector	Voltage (volts)
1	0.850
2	1.35
3	1.52
4	1.56
5	1.25
6	0.985
7	0.032
8	0.029
9	0.027

If they are, the alignment check is completed and the scatterometer is ready to set up for measuring the BRDF of a particular mirror.

Running the BRDF Program

When the computer is first turned on a directory of BASIC programs, text files, and data files will be displayed. A display angle control located on the right side of the computer can be adjusted for optimum viewing of the computer display. To return to the directory from a BASIC program or text file hit the "F8" key. To stop execution of a program at any time press the shift and break keys simultaneously.

Make sure a text file called KFACTR.DO is listed in the directory before running the BRDF program. To run the program, place the black cursor over the directory entry PBRDF.BA and press ENTER. The cursor is moved by pressing one of the arrow keys in the upper right hand corner of the keyboard. Type in the sample ID, date, and number of chopper cycles to sample for each detector as directed by the program. Set the switch on the array housing to "S" for specular samples and "D" for diffuse samples. When ENTER is pressed after entering in the switch setting, the computer will read the detector voltages one at a time consecutively starting with the one farthest from specular. It is recommended that all room lights be turned off while detector signals are being read. The computer will beep once after each detector voltage has been stored, and will beep twice when all data has been collected and the room lights can be turned on again. If desired, save the data in a data file by typing in a file name and whether or not it is to be appended to an existing file as directed by the program (appending files saves directory space). The data can also be printed out on a line printer.

During a data run the BRDF program may display one of two error messages. An error message is given if the laser output fluctuates more than 5% during a data run or when the program autoranging routine has set the amplifier gain to one (the lowest gain available) and the signal is still too high. Take appropriate steps to correct either problem before running the program again.

BRDF Measurements

To measure the BRDF of a particular mirror it is necessary to align the instrument in reference to the surface being measured. The turning mirror, laser, array, and detectors should not be readjusted at this point; adjust only the tripods as outlined below.

1. Place the instrument over the mirror to be measured as shown in Fig. 4. Loosen the tripod post lock screws and adjust the tripods so that the top of the optics rail at the center is about 24 inches above the mirror surface and approximately parallel to it, and the specular beam is incident on the slit at the front of the array sighting tube. Temporarily tighten all tripod post lock screws.

2. Remove the beveled nylon cross hair at the front of the array sighting tube if necessary. Center the beam on the end array element by adjusting the tripods until the maximum signal amplitude is obtained. The procedure for measuring the signal voltage is described in step four of the "Alignment" section above.

Alignment along the vertical axis of the end array element is done by adjusting tripod 1 (see Fig. 5), and along the horizontal axis by adjusting tripods 2 and 3. Note if the top of the optics rail is not the correct height above the sample surface, it may be necessary to adjust all three tripods by the same amount to get the right height and still keep the optics rail parallel to the sample surface.

3. When the beam spot is centered on the end array element, install the beveled nylon cross hair so that the beveled surface faces outward and the cross hair covers the slit near the bottom end. If the specular beam is not centered on the cross hair, readjust the tripods. Remove the cross hair and recheck the alignment on the end array element. Continue in this manner until the specular beam is centered on both the cross hair and the end array element. After adjustment all tripod post lock screws should be tight.

4. Run the BRDF program as described under "Running the BRDF Program".

CALIBRATION OF THE OPTICAL SYSTEM

Calibration of the optical system includes setting up the scatterometer for measurements at a 45-degree incidence angle, aligning the axis of the linear array in the plane of incidence, aligning the detectors for maximum output, and determining BRDF gain factors. The gain factors for each detector and array element are found by dividing BRDF values obtained from Macor on a laboratory scatterometer of known performance by the voltages measured from the Macor on the portable scatterometer. The portable scatterometer BRDF program calculates the BRDF of a given surface by multiplying these gain factors by the measured signals from that surface. The detector angles were calculated by assuming the top of the optics rail was 24 inches above the sample surface and defining the center of the optics rail at 35.95 inches from the end of the rail (Fig. 10).

1. All of the surfaces used in the calibration procedure are mounted so that the surface is one inch above the floor, i.e., the one inch target block, the pentaprism, and the Macor. Therefore, it is necessary to set the top of the optics rail 25 inches above the floor so that it is 24 inches above the sample surface. Adjust the tripods as described in steps one and two in the "Alignment" section above.

2. Check the alignment of the laser as directed in step three in the "Alignment" section above. If the laser is out of alignment loosen the laser support block screws located on the bottom of the optics rail. Re-position the support blocks until the beam is parallel to the optics rail, and re-tighten the support block screws.

3. For a 45-degree angle of incidence at the sample surface the turning mirror must be positioned so that the distance from the center to the point where the laser hits the turning mirror is 29.25 inches as shown in Fig. 10. Remove the turning mirror housing from the optics rail for easier access to the turning mirror. The turning mirror base is adjustable along the axis of the optics rail and is held in place by two screws in the slotted base plate. Position the base so that the outer edge is 5.15 inches from the end (Fig. 10) and the base is approximately parallel to the rail, and tighten the base plate screws.

4. The laser and chopper power can be turned off at this time. Position the plumb bob bracket so that its center is at the center of the optics rail on both sides (points A and B in Fig. 5). Place the one inch thick target block on the floor so that the point of the plumb bob is centered on the cross hair. Remove the plumb bob once the block is positioned.

5. Turn the laser power on and adjust the turning mirror until the beam is centered on the cross hair on the one inch target block. The mirror is adjustable by means of fine pitch adjustment screws on the rear of the mirror mount (Fig. 11). The beam should pass through the top of the optics rail at 24 inches from the center (Fig. 10) and 2 inches from the side; if not some slight adjustments of the turning mirror may be necessary. Install the turning mirror housing.

6. Replace the one inch target block with the pentaprism and prism housing so that the incident beam is approximately centered on the 1/2-inch diameter hole in the metal cover plate of the housing, and the exit beam is reflected upward toward the array. Adjust the position and tilt of the prism, as discussed in step four of the "Alignment" section above, until the exit beam passes through the top of the optics rail 24 inches from the center at the array end of the rail and 2 inches from the side.

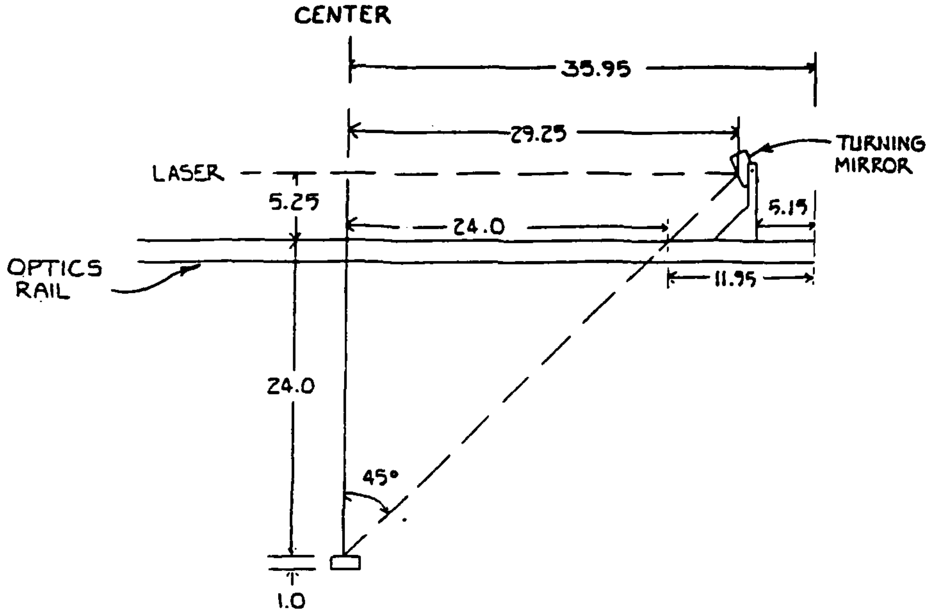

Figure 10.

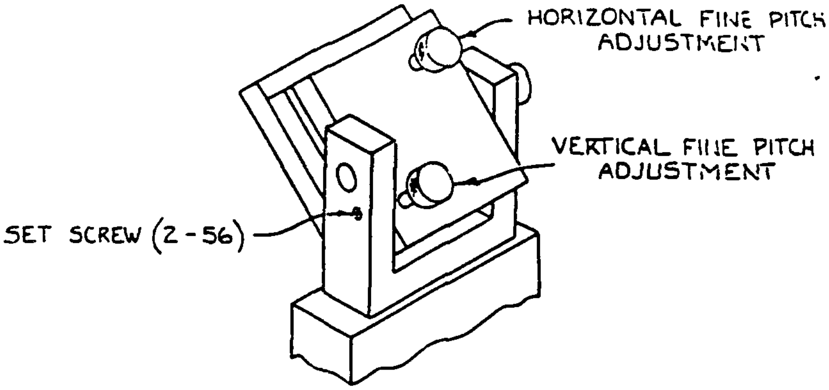

Figure 11.

7. Install the beveled nylon cross hair on the pins next to the slit at the front of the array sighting tube so that the beveled surface faces outward and the cross hair covers the slit near the bottom end. The rotational position of the array assembly within the plane of incidence is held in place by two nuts at the pivot. Adjust the array assembly so that the sighting tube is about 45 degrees from the horizontal and temporarily tighten the pivot nuts.

8. The array assembly is held in place on the optics rail by two screws in the slotted base plate. Due to the twist in the optics rail it may be necessary to put shims under the base plate so that the array assembly will be level. If it is not level, the axis of the array will not be parallel to the plane of incidence which is perpendicular to level surfaces. A circular level placed on the optics rail may be used to determine how much compensation is needed to make the array assembly level. Position the base plate with the shims under it so that the beam is approximately centered on the cross hair and temporarily tighten the base plate screws.

9. Remove the beveled nylon cross hair and measure the signal amplitude of the end array element using the procedure described in step four of the "Alignment" section above (the chopper should be turned on at this time). A lock-in amplifier with the reference signal obtained from the chopper can be used instead of the oscilloscope or voltmeter. Slightly loosen the pivot nuts of the array assembly, adjust the rotational position until the maximum signal from the end array element is observed, and re-tighten the pivot nuts. Slightly loosen the base plate screws, rotate the array assembly side to side for maximum signal, and re-tighten the base plate screws.

10. Replace the beveled nylon cross hair. If the beam is not centered on the cross hair slightly loosen the base plate screws and re-position the array assembly. Remove the cross hair and repeat step nine. Continue in this manner until the beam is centered on both the cross hair and the end array element. Then check the signal from the next array element to be sure it is smaller than the signal from the end element as discussed in step four of the "Alignment" section above.

11. The chopper frequency should be 5 Hz. If not, adjust the frequency dial on the chopper power supply; a setting of approximately 28 produces a 5 Hz chopper frequency. Reconnect the array signal cable to the front panel of the main electronics cabinet.

12. Adjust the nine detector assemblies for maximum signal amplitude at each output as follows. For each detector, disconnect the signal cable from the electronics cabinet and connect it to an oscilloscope or lock-in amplifier (the chopper should be on at this time). Loosen the four screws holding the detector in place on the optics rail, adjust the position of the detector assembly until the maximum signal is observed, and re-tighten the screws. Loosen the pivot nuts and screws slightly (Fig. 12) so that the detector housing is turnable but not loose. Slowly rotate the detector housing to obtain the maximum signal, and re-tighten the pivot nuts and screws. Reconnect the detector signal cable to the front panel of the main electronic cabinet.

13. When the signal of all nine detectors has been maximized, run the BRDF program as described above with the Macor sample and save the data. Return to the directory and place the cursor over KGENER.BA and hit ENTER. This program calculates the gain factors for each detector and array element and stores them in the KFACTR.DO file used by the portable scatterometer BRDF program. It requires the voltages measured by each detector and array element from the Macor sample and these may be enter from the newly created data file or manually from the keyboard.

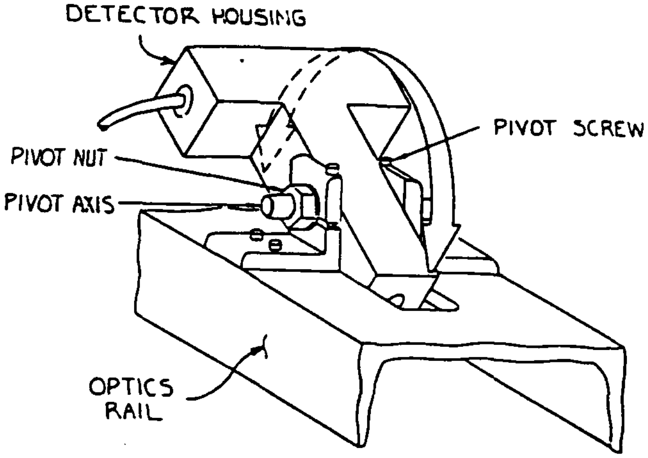
DETECTOR HOUSING
PIVOT SCREW
PIVOT NUT
PIVOT AXIS
OPTICS RAIL

Figure 12.

14. Rerun the BRDF program with the Macor sample with the new gain factors. The BRDF should be about $1/\pi$ at all detector and array element angles.

APPENDIX D

Near-specular Performance of a Portable Scatterometer

Kathleen A. Magee and William L. Wolfe

University of Arizona
Optical Sciences Center
Tucson, Arizona

Abstract

A helium-neon portable scatterometer that was built and described previously has been modified. The intent was to obtain better data at angles very close to specular. We incorporated a twelve-element, linear array of silicon detectors in place of the first detector near the specular reflection direction, and removed the collimator to reduce the beam diameter. Attention was paid to scattered light from the instrument. A new scheme to orient the instrument to the sample surface using the array and the specular beam is described. Design details of the detection system capable of detecting signals ranging over five orders of magnitude and utilizing lock-in detection software are given. Results showing that the modification improved the scatterometer performance so that a Bidirectional Reflectance Distribution Function (BRDF) value of 1 sr^{-1} at one degree from specular can be measured with reasonable accuracy for a specular sample are discussed.

Introduction

As optical systems become more sophisticated the effects of light scatter from optical components on system performance becomes increasingly important, especially at angles very close to specular. A helium-neon portable scatterometer capable of measuring the Bidirectional Reflectance Distribution Function (BRDF), that characterizes scatter from component surfaces, was built and described in an earlier paper[1]. The previous configuration is shown in Fig. 1. The output of a Hughes Series 3000 helium-neon laser (0.6328μm) was collimated, chopped at a frequency of 5 hz, and reflected to the sample surface by a folding flat shown on the right. Instrument orientation to the sample surface was done by centering the specular beam in the sight at the far left. Ten hybrid silicon photodetector/amplifiers each mounted at the end of sighting tubes were placed at various angles between the source and specular beam; the first four near specular were equipped with apertures, the other six with lenses. A Radio Shack TRS-80 Model 100 Portable Computer was used to gather and process the signals from the ten detectors. This portable instrumentation was capable of measuring scatter from diffuse and specular samples up to two meters in diameter at 0.6328μm for a 45 degree incident angle over a fairly large range of scatter angles. However, measurements were limited to a minimum angle from specular of 1.5 degrees which corresponds to a $\beta-\beta_o$ of 0.019 where $\beta-\beta_o$ is the surface spatial frequency times the wavelength over 2 .

This paper discusses the addition of a twelve-element, linear array of silicon detectors placed near the specular beam to obtain better BRDF data in the region near specular.

Modification Details

We modified the scatterometer by replacing the sight and the detector closest to specular with the array assembly. The modification is shown in Fig. 2. The collimator at the output of the laser was also removed to reduce the specular beam diameter at the array from 14mm to 4.5mm. Design considerations that arise as a result of the modification are the field of view of each array element, the scattered light from the instrument, instrument alignment to the sample surface now that the sight has been removed, and the need for a fairly large detector dynamic range.

The field of view of the array elements is defined by a 27mm X 3.6mm slit placed on the end of the array sighting tube. This provides a rectangular field of view at the sample with a minimum dimension of 10.4mm in the direction normal to the plane of inci-

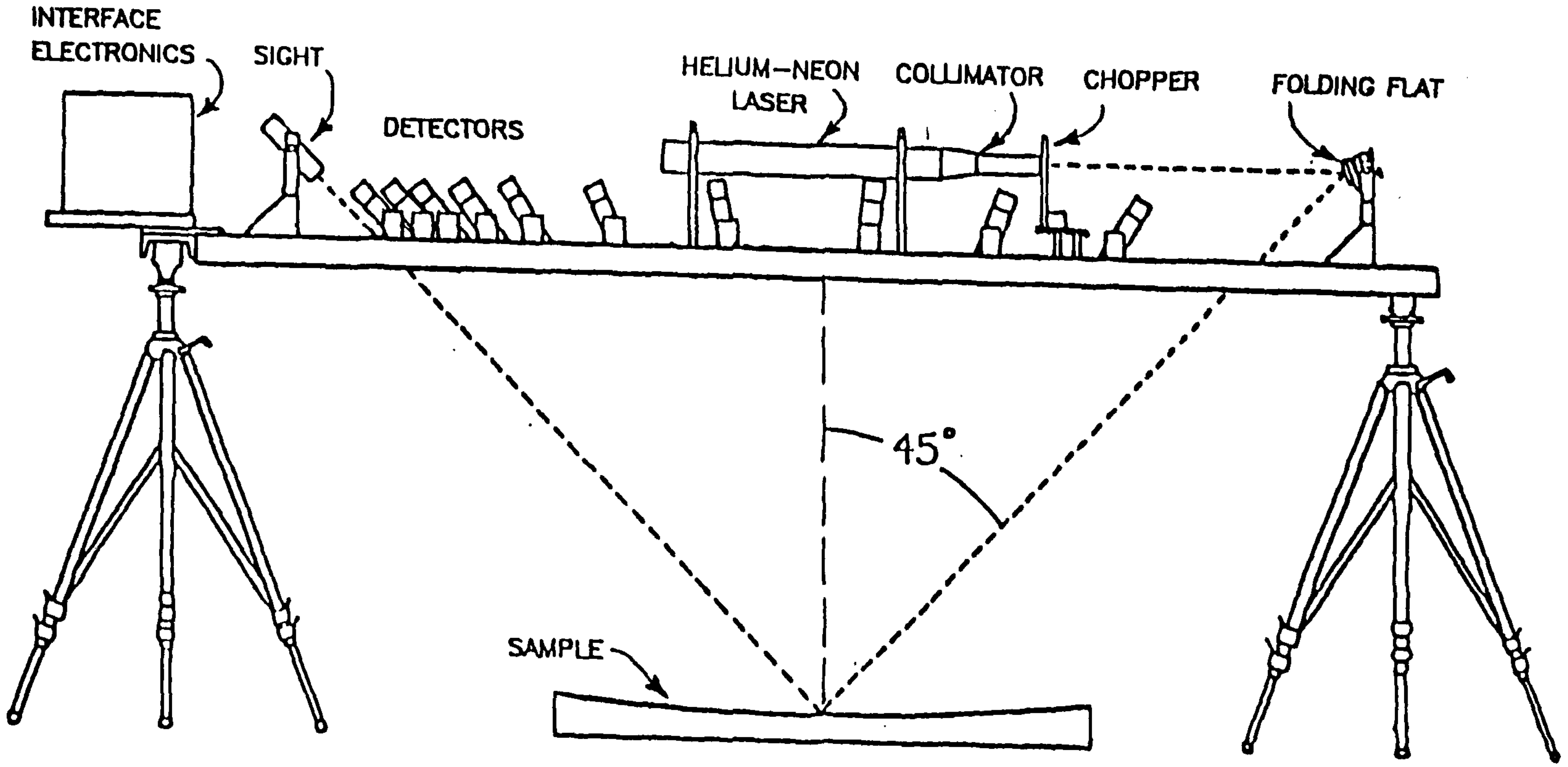

FIGURE 1 Previous scatterometer configuration

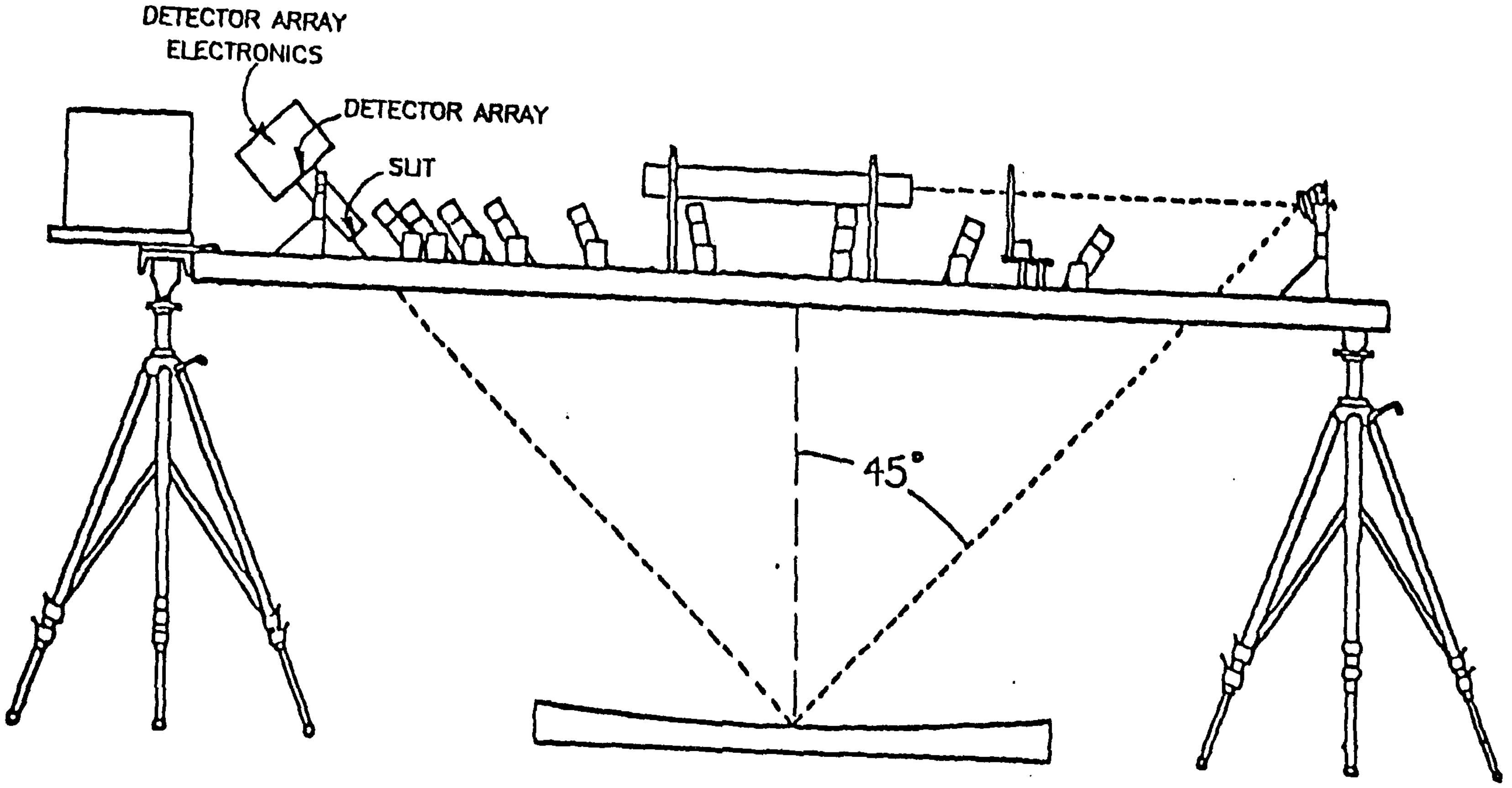

FIGURE 2 Scatterometer modification

dence for each array element. This field of view is fairly large but the signal-to-noise ratios near specular should generally be high, and attention was paid to scattered light from the instrument. To minimize this scatter we replaced the folding flat with a smoother mirror and covered all reflective parts of the instrument.

Since the detector array replaced the sight used for instrument orientation to the sample surface, we incorporated the array in the new alignment scheme. Previously, the specular beam was centered on crosshairs at both ends of a sight that was set at 45 degrees in the instrument angular coordinate system. This alignment insured that the angle of incidence on the sample was 45 degrees and the detectors were in the plane of incidence at specified angles. The new arrangement is based on the same principle. The array assembly is set at 45 degrees and the beam is centered on a removable crosshair placed in the slit at the front. At the other end of the sighting tube the beam is centered on the end array element.

Detection System

The detector array hardware includes a preamplifier for each of the twelve array elements, an Analog Devices 7506 16-channel analog multiplexer, a Burr Brown programmable-gain-amplifier, and an Intersil 7109 integrating A/D converter. A block diagram is shown in Fig. 3. Early tests showed signals gathered from the array with a highly diffuse sample and with a low scatter mirror ranged over five orders of magnitude. This range was too large to maintain both linearity over the entire range and accuracy from the A/D converter at low signal levels. We designed the preamplifiers to maintain linear operation over the desired range and used the programmable-gain-amplifier to provide more gain at low levels. In addition, a switch is provided to manually increase the gain on the preamplifiers for the first three array elements off specular when measuring diffuse samples and decrease the gain for specular samples. Control of the A/D converter, the multiplexer, and the programmable-gain-amplifier is done via ports available in the TRS-80 Model 100 computer.

We used a software approach to lock-in detection to minimize cost and increase instrument portability. Each detector signal is sampled over several chopper cycles. The computer monitors the chopper and repetitively adds signals sampled while the chopper is open and subtracts while the chopper is closed. The software ensures that the number of additions equals the number of subtractions and thus the noise averages to zero while the signal just keeps adding. The signal total is then divided by the num-

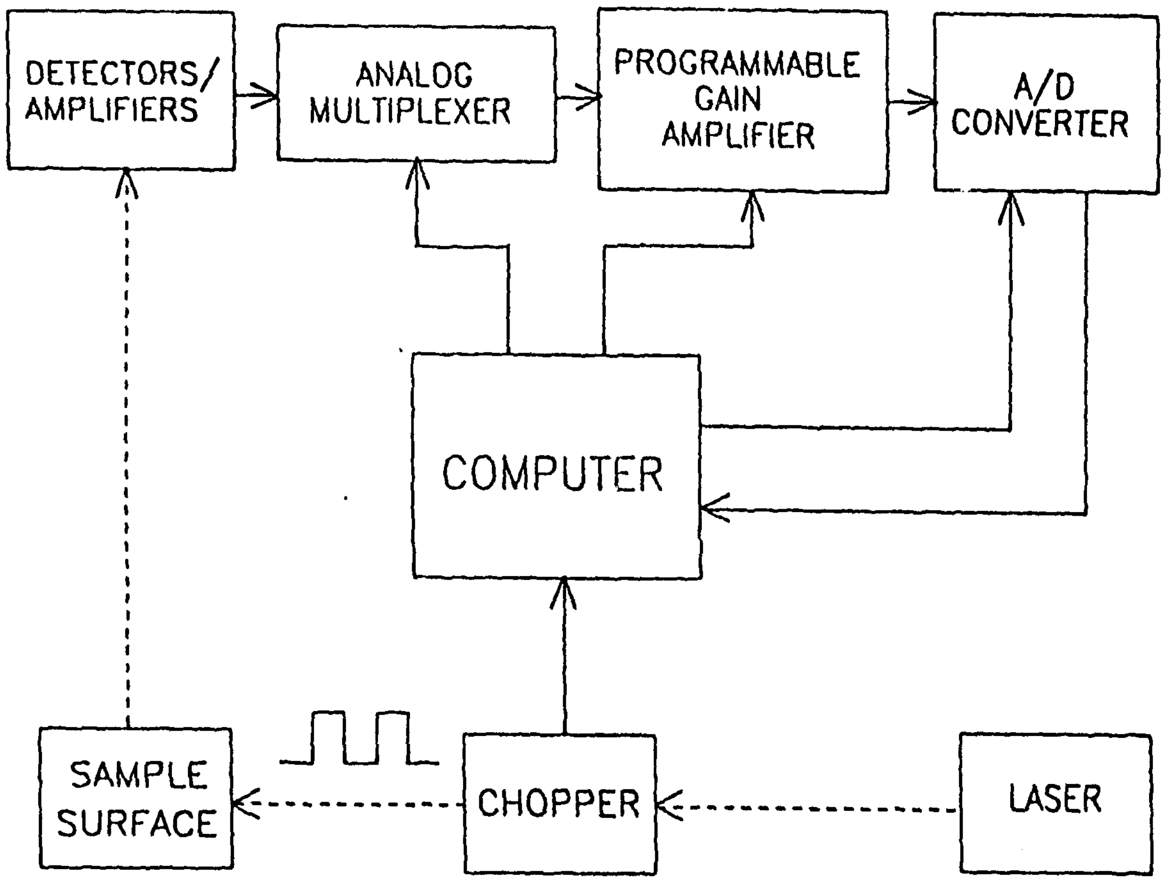

FIGURE 3 Block diagram of the detection system

ber of cycles sampled. The lock-in portion of the system software is written in 8085 assembly language in order to convert and add or subtract signals within a half cycle of the chopper frequency.

Results

Demonstration of performance at near-specular angles and relatively low BRDF values is difficult. We approached this in several steps. The first was to measure Macor, essentially a perfect isotropic sample. The result as shown in Fig. 4 is 1/ "all across the board." The data points between $\beta-\beta_o = 0.001$ and $\beta-\beta_o = 0.015$ were obtained from the array while the other nine points were from the remaining detectors. The next step was to measure one of our best mirrors, a mirror made some time ago by Jaeger, and compare it with the instrument profile. The profile was measured by setting the instrument in a transmission arrangement with no sample as shown in Fig. 5., and is represented by the crosses in Fig. 6. There is a strong indication that the profile drops rapidly near $\beta-\beta_o = 0.01$. The points further out are the noise equivalent BRDF (NEBRDF); the last six points were obtained from detectors equipped with lenses producing a larger collecting area and thus a lower NEBRDF. Under the conditions of measurement (45 degrees incident, 0.6328μm) the mirror still looks good as shown by the circles in Fig. 6. Notice that from $\beta-\beta_o = 0.045$ (3.5 degrees) to larger angles the BRDF is a straight line with a slope of about -2. This agrees with our expectations. Starting at $\beta-\beta_o = 0.015$ (1.2 degrees) the curve is higher and no longer fits the same slope, but closely matches the instrument profile. It has a value of $1\,sr^{-1}$ at one degree. Next, a second inferior mirror was measured and compared with the instrument profile. As shown in Fig. 7 this curve is higher with a slope of about -2 that rolls over at 0.012 and crosses the instrument profile at around 0.004 (0.3 degrees), although there may be some contribution starting at 0.01 (0.8 degrees).

Conclusion

The new configuration reduced the instrument background profile to the point where a BRDF of $1\,sr^{-1}$ can be measured with reasonable accuracy at one degree from specular.

Acknowledgements

We would like to acknowledge the support of the U.S. Air Force (contract number F30602-83-K-0151), Lt. Michial Rau and Lt. Carol Moreland, the mechanical design contributions of Langford G. Brod, and the advice of Dr. James M. Palmer on the electronic and software design.

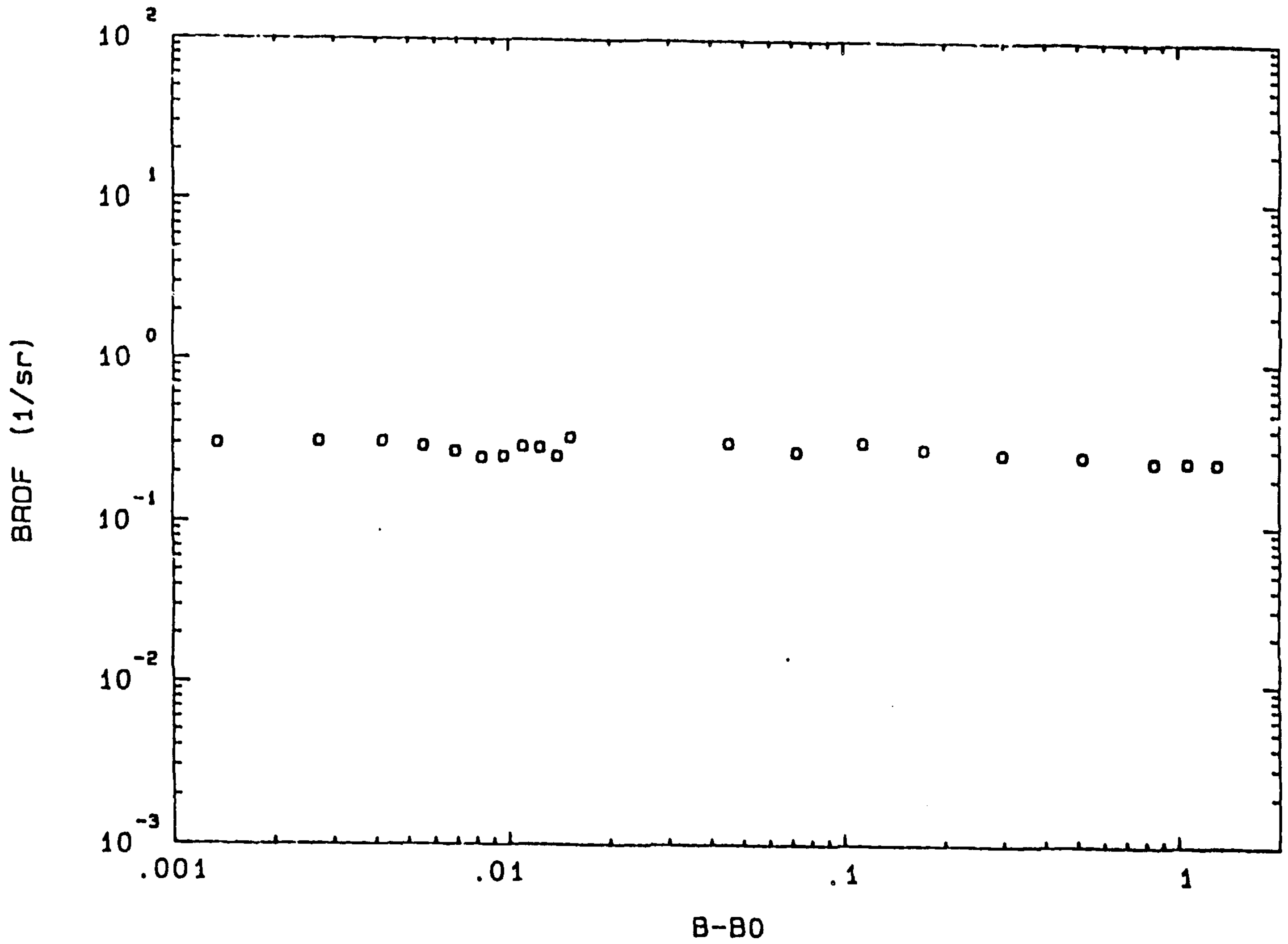

FIGURE 4 BRDF of Macor

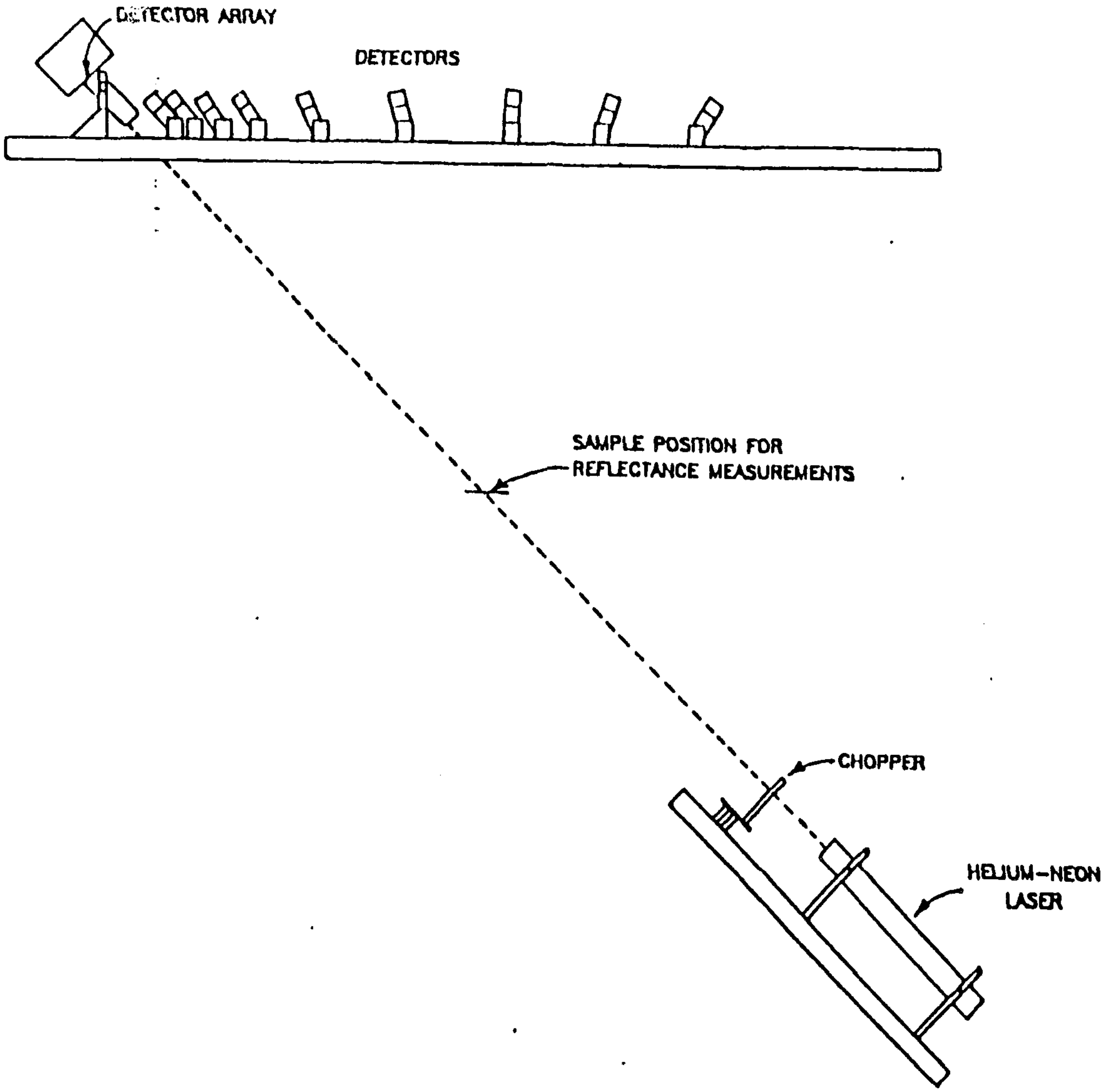

FIGURE 5 Transmission arrangement for measuring the instrument profile

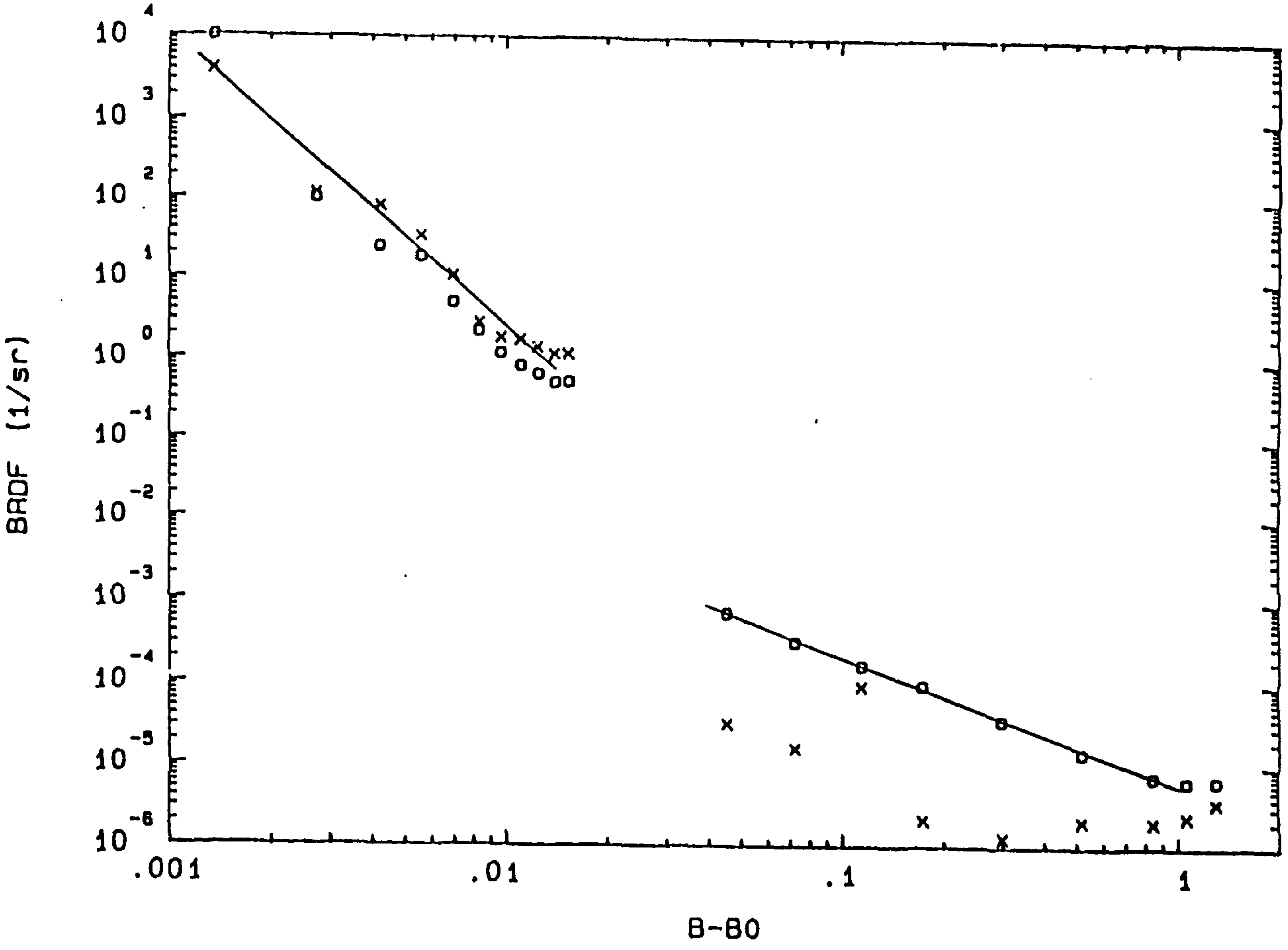

FIGURE 6 Comparison of the Jaeger mirror BRDF with the instrument profile (O–mirror, X–profile)

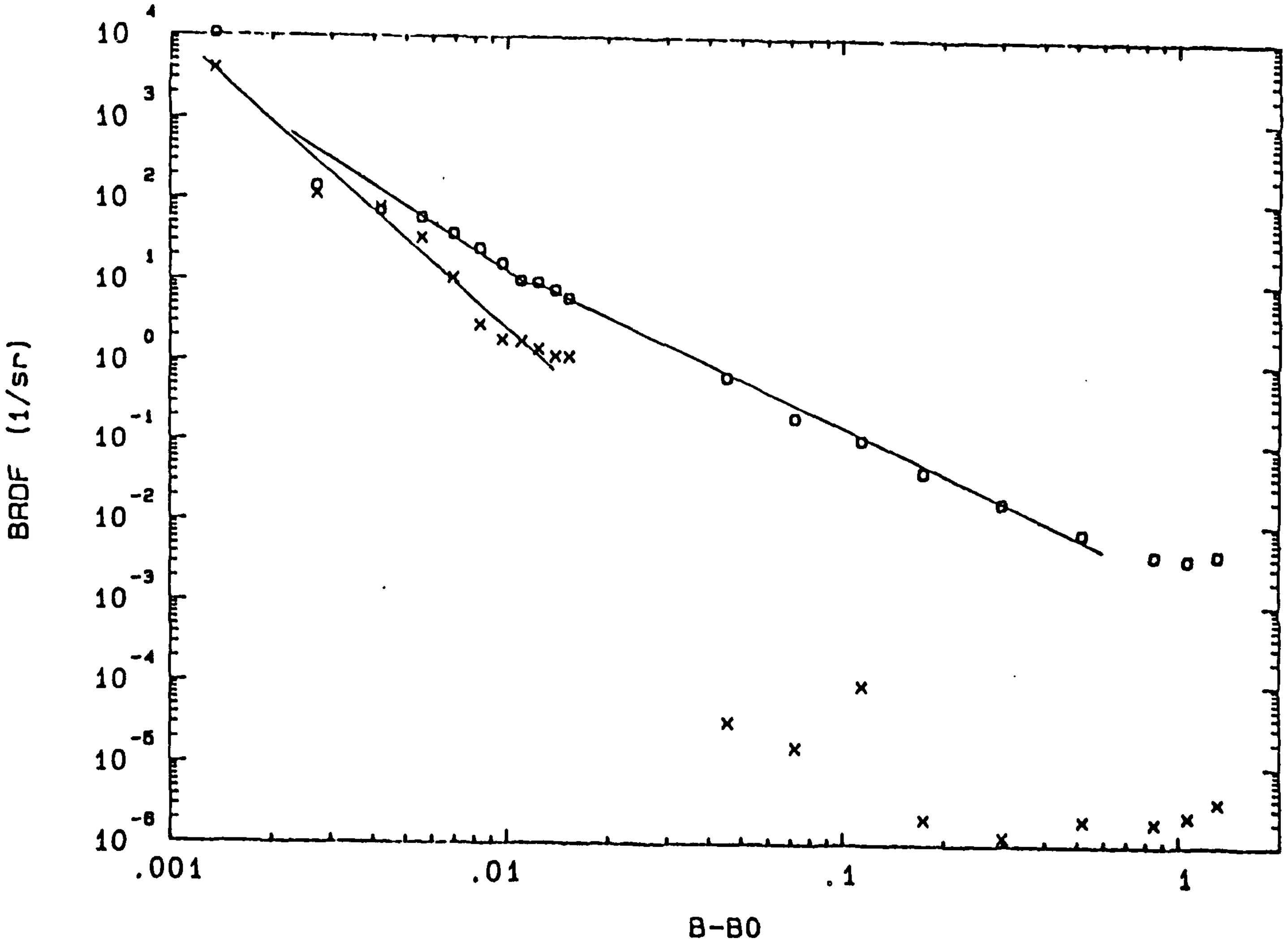

FIGURE 7 Comparison of a second inferior mirror BRDF with the instrument profile (O–mirror, X–profile)

Reference

1. Wolfe, W. L., K. A. Magee, and D. W. Wolfe, "A Portable Scatterometer for Optical Shop Use," Proc. SPIE 525 (1985).

APPENDIX E

A 10.6 μm Portable Scatterometer for Optical Shop Use

Steven J. Wein and William L. Wolfe

INTRODUCTION

We have bread-boarded and tested a design for a 10.6-μm portable scatterometer which can test mirrors up to 1.7 meters in diameter with the emphasis on obtaining near-specular measurements. We have obtained and verified a design that can measure scattering from 2^0 off specular to 80^0 off specular. Near specular the NEBRDF (noise equivalent bidirectional reflectance distribution function) is 10^{-4} sr^{-1} and far off specular the NEBRDF is approximately 10^{-6} sr^{-1}.

The system consists of a 7.5-W CO_2 laser whose beam is expanded and focused by a zinc selenide beam expander. A He-Ne laser beam is coalligned with the infrared beam for aid in alignment and safety purposes. We utilize pyroelectric radiometers to detect the scattered radiation.

The configuration depicted in Figure 1 was chosen on the merits of portability and compactness. The requirements of portability place special constraints on the geometry of the set-up which also affect the near specular performance (which will be subsequently discussed). In addition, this instrument is intended to be able to test many different mirrors with a wide range of radii of curvature. Therefore, in general, we cannot rely upon the power of the test surface to aid in the reduction of the focal spot diameter. We are able to make BRDF measurements to 2^0 from specular when testing a flat mirror. When testing a mirror with positive power, we can make measurements inside 2^0 depending on the power of test surface. On the other hand, we cannot quite obtain 2^0 from specular when testing a surface with negative power.

OPTICAL PATH LENGTH

The above design results in two conflicting requirements on the length of section B. The first requirement is to minimize the focal spot diameter. In order to do this, the system f/# must be reduced; hence, section B must be reduced in length. The second requirement is to minimize the system scattering. To do this the illuminated portion of the turn mirror must be outside the field of view (FOV) for all the radiometers. Especially for the near specular radiometer this requires an increase in the length of section B. On paper, there is a region that satisfies both of these conditions. For our geometry, both conditions are theoretically satisfied for 1^0 off specular when section B of Figure 1 is 1.94 meters or slightly greater. (Unfortunately, this is rather large to satisfy the portability requirement.) Both conditions are satisfied for 1.8^0 off specular when section B is approximately 60 cm. However, this assumes that the baffle of the radiometer stops all off-axis radiation and that the specular beam falls off as a Gaussian beam over orders of magnitude from the peak irradiance. Both are dubious assumptions. In practice we have found that the roll-off of the beam profile is sufficiently low and the baffle of the radiometer is sufficiently "black" at 2^0 from specular to obtain BRDF measurements of 10^{-4} sr^{-1}.

In addition, section A should be short enough to yield an acceptable signal-to-noise ratio (SNR) for a BRDF of 10^{-4} sr^{-1}. However, section A should also be long

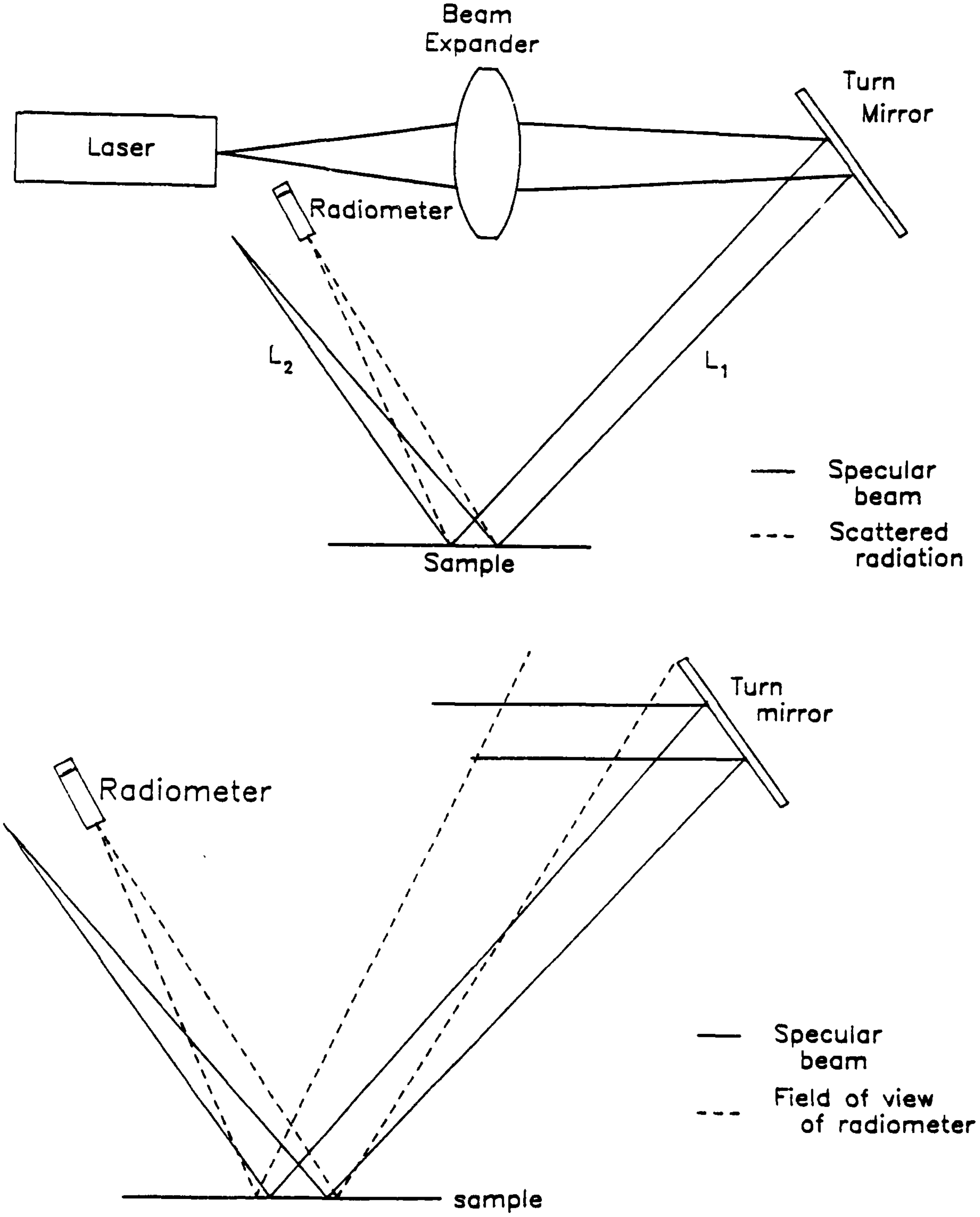

Figure 1. Top: Geometrical layout. Bottom: System scatter vignetted from radiometer's field of view.

enough that the separation between the specular beam and 2^0 is large enough for the specular irradiance to be below the scattered irradiance.

NEAR SPECULAR BAFFLE

Off-axis stray radiation inside the radiometer is perhaps the predominant problem. Especially, but not exclusively, at two degrees off the axis of the radiometer is a strong noise contribution due to the system scattering and the specular beam.

If we utilize a long baffle radiometer we can forego the need for a higher D^* detector. To obtain a sufficiently small FOV for the radiometer such that it does not see the "illuminated" portion of the turn mirror (which we are defining to be the $1/e^4$ irradiance points) we need to close down the entrance aperture of the baffle. However, for short baffles the aperture becomes sufficiently small such that the power transfer from the sample to the detector yields a signal to noise less than one. The solution to this is to determine the appropriate aperture large enough to allow a sufficient SNR then extend the baffle length to reduce the FOV to be sufficiently narrow. A 3-mm aperture at the end of a 25.4-cm baffle meets the criteria (Figure 2). We placed additional fins inside the baffle as indicated above such that the detector cannot directly see the sides of the baffle. This did reduce the off-axis stray radiation rejection but not sufficiently to make measurements at one degree off specular.

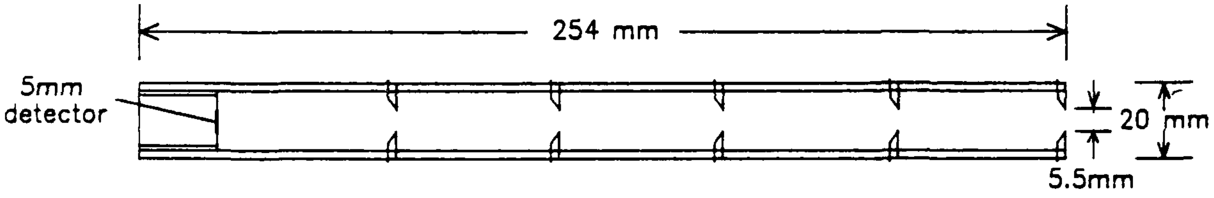

Figure 2. Baffle schematic.

BEAM EXPANDER/FOCUSING ELEMENT

We must significantly underfill the exit pupil of the system to maintain the Gaussian roll-off of the focal spot. The truncated beam will very nearly resemble a Gaussian beam until the point of truncation where we obtain ringing in the diffraction pattern that falls off as $1/r^3$.

The exit pupil diameter of our zinc selenide beam expander is 23 mm and the $1/e^2$ diameter of the Gaussian beam at the exit pupil is 7.5 mm. Hence, the beam is truncated just below the $1/e^{18}$ level and theoretically maintains the Gaussian roll-off until just reaching the scattering level. This was verified by first obtaining a signal voltage due to a gold sandpaper Lambertian surface. Then an rms noise voltage was obtained while the laser was operating and all the optical and electrical noise mechanisms where active. We obtained a ratio of 3000 between the two measurements which is what was required to obtain a 10^{-4} BRDF measurement at that location.

Spatial filtering of the beam with a Keplerian type beam expander improves the system performance such that we are able to make measurements to 1.60^0 off specular. However, the diameter of the pinhole is very important. If the pinhole is too small, the diffraction from the pinhole can fill the exit pupil. If the exit pupil is fully illuminated with a plane wave for example, the system point spread function will be the Airy diffraction pattern which does not roll off quickly enough to make near-specular measurements. We experimentally determined that the optimum spatial filter diameter for this particular application is approximately 3.5 times the diameter of the focal spot at the $1/e^2$ points. Spatial filters with smaller diameters produced an increase in specular irradiance in the region from one to two degrees from specular.

DETECTION SYSTEM

This system utilizes the Molectron P1-72 and P1-75 lithium tantalate pyroelectric detectors with built-in JFET preamplifiers. These are low-noise pyroelectric detectors with an NEP of 0.5 nW. The use of pyroelectric detectors facilitates portability and ease of operation since cooling is not required. The detectors are operated in a voltage gain configuration and ac coupled into a low noise Burr-Brown OPA111 operational amplifier with feedback set for a closed loop gain of 500. This yields an acceptable signal level for the subsequent A/D conversion and signal processing.

MECHANICAL CHOPPING SCHEME

The chopping of the beam by the chopper blade yields a temporal convolution between the shape of the slots in the chopper blade and the beam cross section. (See Figure 3.) Thus, we can modify the temporal signal as seen by the pyroelectric detectors by appropriately choosing the width and shape of the slots in the chopper blade. At maximum responsivity our pyroelectric detectors are operating in the integrating region of their Bode plot. Utilizing phase sensitive lock-in detection we would like as much as possible of the detector output to be in the fundamental harmonic. Hence, we would like the temporal signal to be as close to a sinusoid as possible. By having the width of the slots (in the direction normal to the

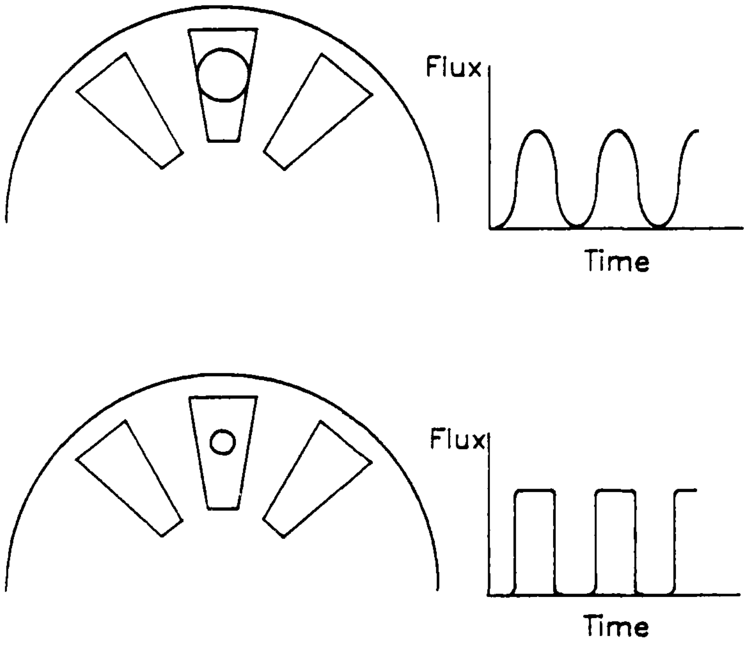

Figure 3. Mechanical chopper convolution.

measurement plane) approximately equal to the $1/e^2$ diameter of the Gaussian beam, the convolution yields a temporal signal that is very nearly sinusoidal when viewed on an oscilloscope. (The other dimension of the slot is necessarily large to avoid additional unwanted diffraction in the measurement plane.)

All results described above were obtained using the Optical Sciences Center Infrared Facility Laboratory. Thus, we have been able to show with laboratory components an instrument configuration that has an instrumental NEBRDF of 10^{-4} sr^{-1} at 2^0 from specular. The next step is the assembly of the components into an operational instrument.

ACKNOWLEDGMENTS

We appreciate the support of the Rome Air Development Center, via contract F30602-83-K-0151 and the comments and suggestions of Lts. Michial Rau and Carol Moreland.

APPENDIX F

Reprinted from Journal of the Optical Society of America, Vol. 73, page 1596, November 1983

Scattering from microrough surfaces: comparison of theory and experiment

Yaujen Wang and William L. Wolfe

Optical Sciences Center, University of Arizona, Tucson, Arizona 85721

Received February 25, 1983

Scattering data taken at 0.6328, 3.39, and 10.6 μm are compared with theoretical calculations based on vector and scalar theories of scattering. Methods are described for obtaining the rms surface height using various degrees of dependence on the models of scattering.

INTRODUCTION

Scattering from almost smooth surfaces is important in some optical systems and in certain radar problems. These surfaces, with roughness less than a wavelength, are realized by well-made mirrors in optics and relatively calm ocean surfaces at longer wavelengths. Calculations of the amount and distribution of the scattering have been made based on both the scalar and the vector approaches to electromagnetic boundary value problems. The scalar theory, based on a scalar diffraction integral, has been developed by Davies,[1] Beckmann,[2] and Harvey.[3] The vector theory, based largely on perturbation or variational techniques or the Stratton–Chu–Silver diffraction integral,[4,5] has been developed by many authors.[6] The perturbation technique was originated by Rayleigh,[7] extended by Rice, and used for the solution of both optical and radar problems.

Although measurements have been made over the years of scattering[8] at various wavelengths[9] and for surfaces of various roughnesses, there seems to have been no systematic comparison of the theory and the data.

We have made measurements of the angular distribution of scattering for three different angles of incidence, five different wavelengths, and several different polarization arrangements, all for a single sample of smooth fused silica with an evaporated aluminum coating. We compared these data with the vector and the scalar models, and we drew some tentative conclusions about the agreement of theory with measurements based on these comparisons.

THEORETICAL BACKGROUND

Classical scalar theory has been used quite successfully to calculate diffraction from obstacles and apertures. Assumptions are made so that the properties of the materials (such as conductivity and dielectric constants) do not enter the calculations. No notice is taken of polarization, but if there exists only a single polarization in the incident beam and ellipticity is not introduced, the problem is a scalar one. For the metallic sample and the angles of incidence that are used, vector theory shows that the ellipticity introduced on reflection is negligible.

Vector theory, using only the first term of the scattered-field expression as described by the references cited,[6] can be written as

$$f_r^{ss} = \frac{1}{P_0}\frac{\mathrm{d}P^{ss}}{\mathrm{d}\Omega} = \frac{1}{\pi^2}k^4F_{ss}W(p), \tag{1}$$

$$f_r^{pp} = \frac{1}{P_0}\frac{\mathrm{d}P^{pp}}{\mathrm{d}\Omega} = \frac{1}{\pi^2}k^4F_{pp}W(p), \tag{2}$$

where

f_r is the bidirectional-reflectance distribution function (BRDF),[10]
P_0 is the incident power,
P is the scattered power,
Ω is the solid angle,
$k = 2\pi/\lambda$,
λ is the wavelength of the radiation,
F is the optical factor (given explicitly below),
$W(p)$ is the power or the variance spectrum of the surface height distribution,
$p = k(\sin\theta_s - \sin\theta_i)$ is the surface spatial frequency,
θ_s is the angle of scatter,
θ_i is the incidence or specular reflection angle with respect to the average surface normal,
ss means that the source and the receiver both are polarized with the electric vector normal to the plane of incidence, and
pp is the equivalent parallel situation.

The vector theory predicts that

$$F_{ss} = \cos\theta_i \cos\theta_s, \tag{3}$$

$$F_{pp} = F_{ss}\left(\frac{1 - \sin\theta_i \sin\theta_s}{\cos\theta_i \cos\theta_s}\right)^2. \tag{4}$$

Scalar theory predicts, for instance, from Davies,[1] that

$$F = (\cos\theta_i + \cos\theta_s)^4/\cos\theta_s. \tag{5}$$

The surface-height spectrum $W(p)$ is the Fourier transform *of the autocorrelation of the surface height distribution.* This is, of course, equivalent to the spectrum of the distribution of the variance from the mean surface height. Many authors have assumed either Gaussian or exponential forms for the autocorrelation function, and these lead to Gaussian or Lorentzian power spectra. We make no such assumption ini-

0030-3941/83/111596-07$01.00

tially. Simple reasoning leads to the conclusion that a two-dimensional power spectrum should be used, but there are reasons for concluding that a one-dimensional spectrum is also valid. Appendix A shows that, in the latter case, k^4 in the BRDF equations should be replaced by k^3.

Since we measured the scattering of unpolarized radiation with an unpolarized receiver as well as the *ss* and the *pp* situations, the theoretical relationships that we used should be given. It is well known that the total flux is given by

$$dP^{uu} = \frac{1}{2}(dP^{ss} + dP^{sp} + dP^{ps} + dP^{pp}). \qquad (6)$$

However, when polarized radiation is obtained from unpolarized radiation with a polarizer pair that has a transmission of either τ_{ss} or τ_{pp}, one has

$$dP^{ss} = \tau_{ss} dP^{uu}, \qquad (7)$$

$$dP^{pp} = \tau_{pp} dP^{uu}. \qquad (8)$$

When these substitutions are made in Eq. (6) the result is

$$f_r^{uu} = \frac{1}{2}(f_r^{ss} + f_r^{pp}). \qquad (9)$$

We have also made use of the fact that the cross terms are theoretically zero and we found them to be experimentally unmeasurable.

The same result is obtained from scalar theory but from different physical reasoning. Since scalar theory treats all polarizations equally, the BRDF is always the average of all the polarization terms. For in-plane measurements the result is given above. However, for out-of-plane measurements the scalar result should be half of the vector result.

EXPERIMENTAL PROCEDURE AND RESULTS

All data were taken on a single sample of well-polished fused silica that had a 70-nm-thick evaporated coating of aluminum on its surface. Such a surface has often been called superpolished. The sample was measured on the Naval Weapons Center Talystep instrument[11] and found to have an rms roughness of about 8 Å (0.8 nm, or 8×10^{-4} μm). The scatterometer used for the measurements has been described elsewhere.[12] Measurements were made at 0.6328, 3.39, and 10.6 μm at angles of incidence of 10°, 30°, and 50° for *ss* and *su* polarization and 0.488, 0.5145, and 0.6328 μm for *pp* polarization. The perpendicular polarizations were not available at the longer wavelengths because of equipment limitations. It is generally true that the data are reliable from $\beta - \beta_0$ ($\sin\theta_s - \sin\theta_i$) values greater than about 0.08 and until the data *curl up* at large angles because of noise or other extraneous effects. Figures 1–5 show representative data and vector-theory curves that are adjusted by the choice of rms roughness and autocorrelation length; Figs. 6–8 show the instrument function and the noise level. We believe that the uncertainty of our measurements is 20% in most cases, al-

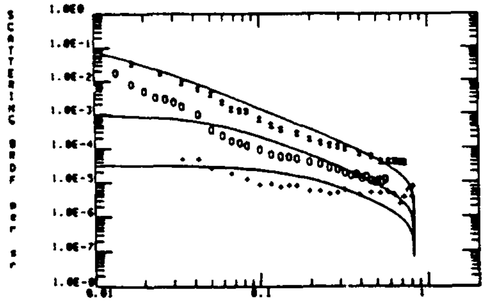

Fig. 1. BRDF data for 0.6328 μm (*), 3.39 μm (0), and 10.6 μm (+) for 10° incidence and the corresponding one-dimensional vector theory (*ss*) (solid lines).

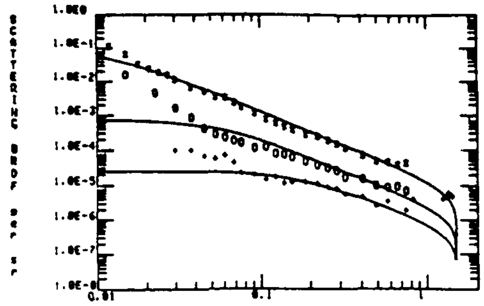

Fig. 2. BRDF data for 0.6328 μm (*), 3.39 μm (0), and 10.6 μm (+) for 30° incidence and corresponding one-dimensional vector theory (*ss*) (solid lines).

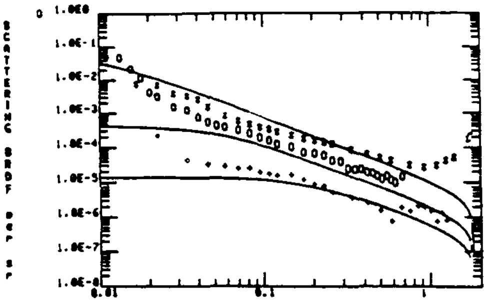

Fig. 3. BRDF data for 0.6328 μm (*), 3.39 μm (0), and 10.6 μm (+) for 50° incidence and corresponding one-dimensional vector theory (*ss*) (solid lines).

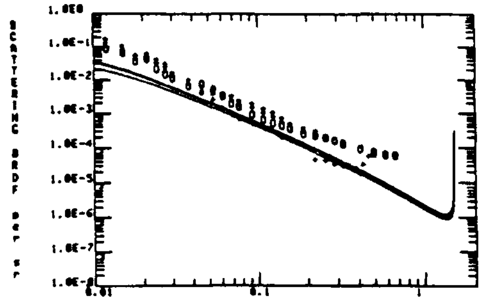

Fig. 4. BRDF data for 0.6328 μm (+), 0.5145 μm (x), and 0.4880 μm (0), and the corresponding one-dimensional vector theory (*pp*) (solid lines) for 30° incidence.

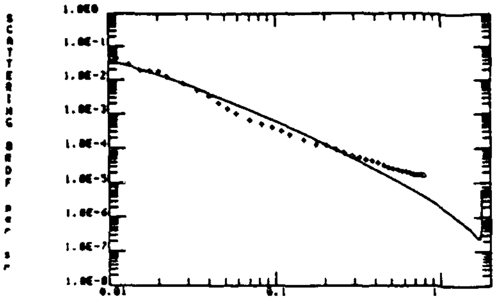

Fig. 5. BRDF for 0.6328-μm unpolarized theory exponential model for 50° incidence.

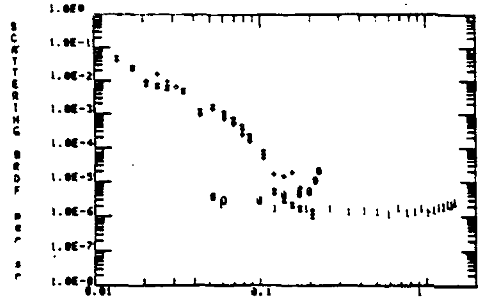

Fig. 6. Instrument function for positive (+) and negative (*) $\beta - \beta_0$ at 0.6328 μm and noise level for positive (θ) and negative (1) $\beta - \beta_0$.

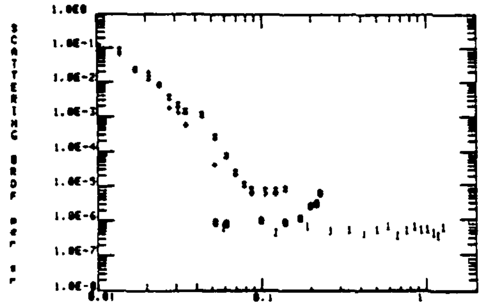

Fig. 7. Instrument function for positive (+) and negative (*) $\beta - \beta_0$ and noise level for positive (θ) and negative (1) $\beta - \beta_0$ at 3.39 μm.

though it can increase when we approach the noise at low values of BRDF and at high or low values of $\beta - \beta_0$.

RESULTS

One of the most satisfying ways of comparing the data and the theory is to calculate the surface height spectrum from the BRDF data and the theoretical relationship. In general, this means that

$$W_2(p) = f_r \Big/ \left(k^4 F \frac{1}{\pi^2}\right). \tag{10}$$

$$W_1(p) = f_r \Big/ \left(k^3 F \frac{2}{\pi}\right). \tag{11}$$

The radian wave number is raised to either the third or the fourth power, depending on the assumption of a one-dimensional or a two-dimensional power spectrum. The factor F is taken from the appropriate theory. Nothing more is assumed about either $W(p)$ or the data.

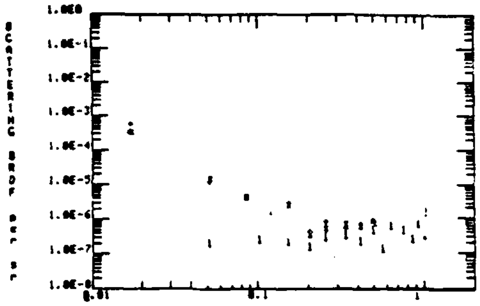

Fig. 8. Instrument function for positive (+) and negative (*) $\beta - \beta_0$ and noise level for negative $\beta - \beta_0$ at 10.6 μm.

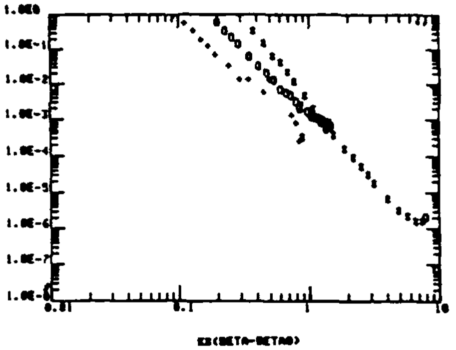

Fig. 9. Power spectrum for 0.6328, 3.39, and 10.6 μm at 30° incidence with two-dimensional Beckmann model.

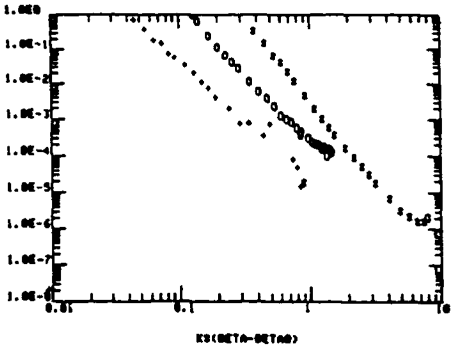

Fig. 10. Power spectrum for 0.6328, 3.39, and 10.6 μm at 30° incidence with one-dimensional Beckmann model.

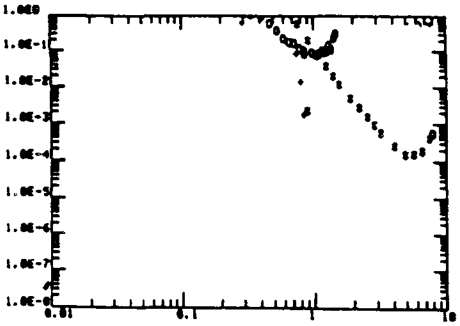

Fig. 11. Power spectrum for 0.6328, 3.39, and 10.6 μm at 30° incidence with two-dimensional Davies model.

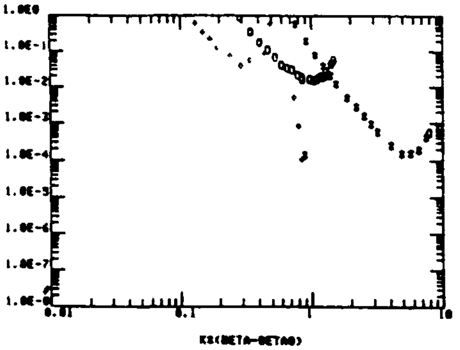

Fig. 12. Power spectrum for 0.6328, 3.39, and 10.6 μm at 30° incidence with one-dimensional Davies model.

Figure 9 shows the result of calculating $W'_2(p)$ using a two-dimensional Beckmann model. Three different spectra for the actual (unique) surface-height distribution are obtained. This is clearly unsatisfactory. Figure 10 shows a similar situation for the Beckmann one-dimensional model. The Davies model preceded that of Beckmann. Both are scalar and both are unsatisfactory, as Figs. 11 and 12 demonstrate.

Figure 13 shows the situation for the vector theory with a two-dimensional power spectrum. Although it is a better fit, the three curves are different by about an order of magnitude in the central portion of the curve. A typical experimental uncertainty is about the size of the markers (0, *, +) showing the data points. Figure 14 is very satisfying. The 10-μm data are indicated by a + and extend almost to $p = 1\ \mu m^{-1}$. In that region they curl up. This is due to experimental noise effects. Similar but less-pronounced effects occur for 3.39-μm data a little beyond $p = 1$ and for 0.6328-μm data at about $p = 7$. In the region from $p = 0.1\ \mu m^{-1}$ to $p = 1\ \mu m^{-1}$, where all the curves overlap, they all predict the same surface-height distribution—a straight line with a slope that is approximately −2. The 0.6328-μm data extend the same line about another order of magnitude in p. The other end of the curve has some difficulties associated with it. The 0.6328- and 3.39-μm data seem to extend to shorter values of p with the same slope, whereas the 10-μm data tend to *roll over*. Unfortunately this is the region in which the measured data are contaminated with scattering from the instrument near the specular direction. Note that $p = 0.5\ \mu m^{-1}$ corresponds to $\beta - \beta_0 = 0.05$, 0.27, and 0.84 for 0.6328, 3.39, and 10.6 μm, respectively. Instrument scatter generally starts at about $\beta - \beta_0 = 0.07$ (and influences measurements at shorter values), but the influence on the measurement is a function of the absolute value of the measurement. A theoretical curve is also shown in Fig. 14. It is a one-dimensional Lorentzian derived from an exponential correlation function and fitted to our data. The rms surface height σ and the correlation length l were found to be 33.5 Å and 10 μm, respectively. This theoretical curve fits our reliable data well, but other spectra could be used.

Figures 15–19 are similar curves for other angles of incidence. Some of the fits are not so good, but we believe that they all support the one-dimensional vector theory quite well. Figure 20 shows similar data for *pp* polarization but for three shorter (and more similar) wavelengths, and Fig. 21 shows that of *uu* (un)polarization. Both are very close to the *ss* 0.6328-μm power spectrum. The data support the conclusions earlier stated.

Another approach was taken to assess the validity of the Lorentzian spectrum. We assumed that $W_1(p)$ was Lorent-

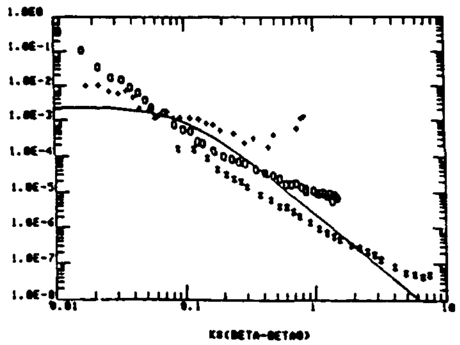

Fig. 13. Power spectrum for 0.6328, 3.39, and 10.6 μm for 30° incidence with two-dimensional vector theory and corresponding theoretical curve (solid line).

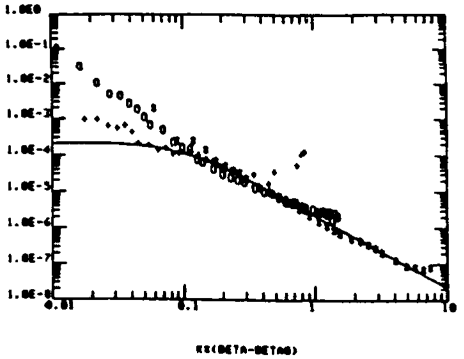

Fig. 14. Power spectrum for 0.6328, 3.39, and 10.6 μm for −30° incidence with one-dimensional vector theory and corresponding theoretical curve (solid line).

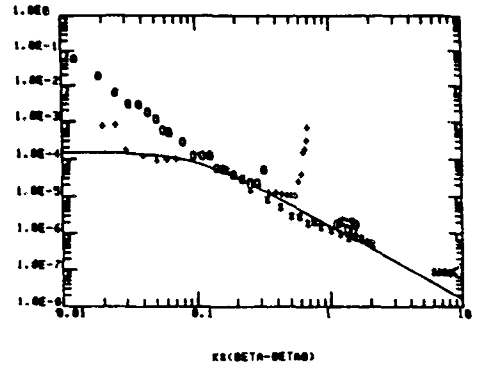

Fig. 15. Power spectrum for 0.6328, 3.39, and 10.6 μm for −10° incidence with one-dimensional vector theory and corresponding theoretical curve (solid line).

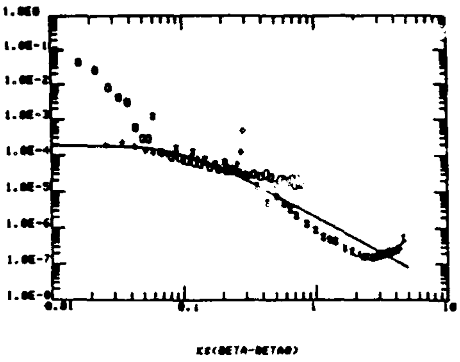

Fig. 18. Power spectrum for 0.6328, 3.39, and 10.6 μm for 30° incidence with one-dimensional vector theory and corresponding theoretical curve (solid line).

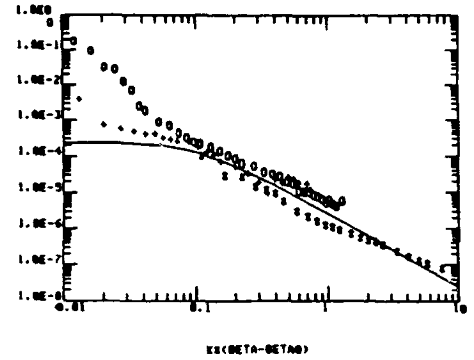

Fig. 16. Power spectrum for 0.6328, 3.39, and 10.6 μm for −50° incidence with one-dimensional vector theory and corresponding theoretical curve (solid line).

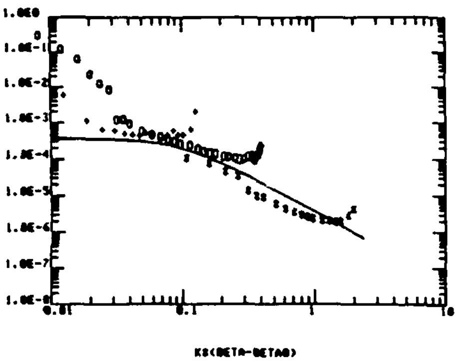

Fig. 19. Power spectrum for 0.6328, 3.39, and 10.6 μm for 50° incidence with one-dimensional vector theory and corresponding theoretical curve (solid line).

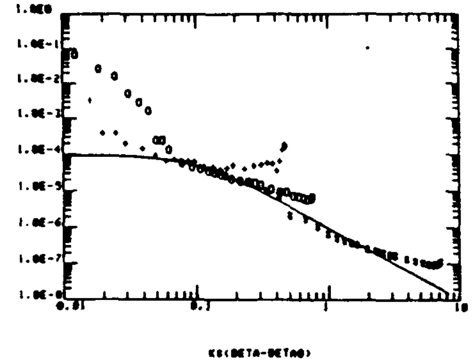

Fig. 17. Power spectrum for 0.6328, 3.39, and 10.6 μm for 10° incidence with one-dimensional vector theory and corresponding theoretical curve (solid line).

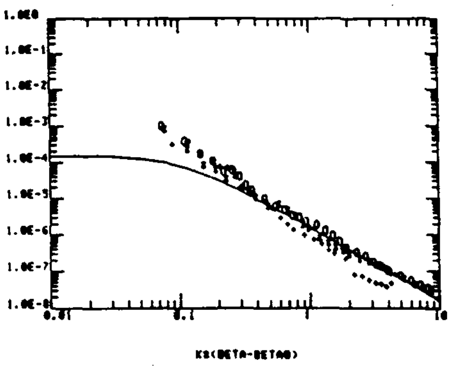

Fig. 20. Power spectrum for 0.488, 0.5145, and 0.6328 μm at 30° incidence with one-dimensional vector model and corresponding theoretical curves.

zian, and we calculated σ and l. Table 1 shows these results for σ obtained by using vector theory. The correlation length was found to be constant at 12 μm. For *ss* data three values for σ were obtained: 27, 40, and 50 Å. For *pp* data three values were found: 13, 19, and 25 Å. For *uu* data three values were found: 11, 15, and 16 Å. These were all found by curve

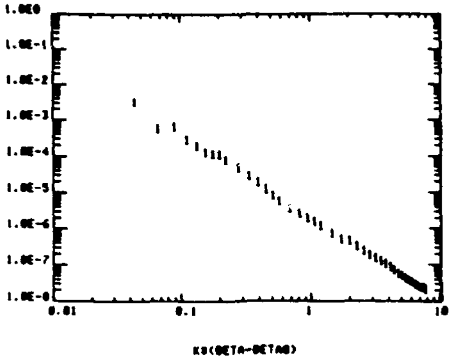

Fig. 21. Power spectrum for *uu* polarization at 30° incidence based on one-dimensional vector model.

fitting. Table 2 shows similar results when scalar theory is used.

The *pp* values are about half of those obtained from *ss* data and vector theory. We are told that this is not unusual. The *uu* data agree well with the *pp* and with the scalar-theory results.

Table 3 shows results obtained by curve fitting the derived $W(p)$ results and by integrating under these curves. We would expect the σ values for a given angle of incidence to be the same whether they were obtained by fitting BRDF or surface spectrum data. The integrals are obtained by adding the area under the power spectrum piece by piece. Some differences should arise from this approximation.

The rms surface height obtained for *ss* vector theory is about 3–4 nm. When obtained by using *pp* data it is about 2 nm. When obtained by using scalar theory it is about 1.5 nm. Independent measurements by Bennett[11] using a surface profilometer give 0.8 nm, as do the results of Wyant using a heterodyne interference microscope.[13]

DISCUSSION

It should be emphasized that all these results are for an exhaustively measured single sample.

The series of curves of $W(p)$ versus p shows clearly that only the one-dimensional vector theory is a reasonable model for scattering regardless of the form of $W(p)$. There is at present no explanation for the discrepancy between *pp* and *ss* data in predicting σ, although our *pp* data were limited in wavelength range. The agreement, or lack of it, among the several different methods of obtaining σ is disturbing. It seems to indicate that the connection between the BRDF and the surface properties has not been completely established.

The set of $W_1(p)$ curves using one-dimensional vector theory provides encouraging evidence for wavelength and angle scaling for values of p larger than $1/l$, in spite of the incomplete theoretical verification.

The next steps for investigation are *pp* data for a larger-wavelength region and more-reliable measurements for smaller values of $\beta - \beta_0$. It seems obvious also that other samples should be investigated.

APPENDIX A. TRANSITION FROM TWO-DIMENSIONAL TO ONE-DIMENSIONAL POWER-SPECTRA EXPRESSIONS

From Eq. (1), the two-dimensional BRDF can be expressed as

$$f_r{}^{ss} = \mathrm{BRDF} = \frac{1}{\pi^2} k^4 \times F_{ss} \times W_2(p). \tag{A1}$$

The power spectrum $W_2(p)$ is the Fourier transform of autocorrelation function $g(\tau)$. If the surface is assumed to be isotropic, and the exponential autocorrelation function is also assumed, the explicit form of Eq. (1) is

$$f_r{}^{ss} = \frac{1}{\pi^2} k^4 \times F_{ss} \int_{-\infty}^{\infty} \int_{-\infty}^{\infty} \sigma^2 \exp[-(x, y)/l] \times \exp[-j2\pi(xf_x + yf_y)] \mathrm{d}x\, \mathrm{d}y. \tag{A2}$$

Table 1. Values of rms Surface Height for Different Measurements Obtained with Vector Theory (in angstroms)

Incidence Angle (deg)	Wavelength *ss* 0.6328	*ss* 3.39	*ss* 10.6	*pp* 0.6328	*pp* 0.5145	*pp* 0.4880	*uu* 0.6328
−10	27	41	41	25	25	25	15
+10	27	27	27	25	25	25	
−30	41	41	41	19	19	19	16
30	41	41	41	19	19	19	11
−50	27	50	41	13	13	13	
50	27	27	27	19	19	19	

Table 2. Values of rms Surface Height Obtained by Fitting Scalar Theory to BRDF Data

Incidence Angle (deg)	Wavelength *ss* 0.6328	*ss* 3.39	*ss* 10.6	*pp* 0.6328	*pp* 3.39	*pp* 10.6	*uu* 0.6328
−10	8	12	10	8	9	9	8
10	9	8	8	8	9	9	5
−30	11	15	13	8	10	9	7
30	13	13	11	10	11	11	8
−50	15	16	13	13	15	16	11
50	16	18	21	18	16	18	11

Table 3. Values of rms Surface Heights Obtained from the Vector Theory by (A) Integration and (B) Curve Fitting to $W(p)$

Incidence Angle (deg)	A	B
−10	21	28
10	17	23
−30	24	34
30	20	31
−50	32	35
50	32	43

where $\exp[-(x, y)/l]$ is the two-dimensional exponential autocorrelation function. If it is separable, $\exp[-(x, y)/l]$ is equal to $[\exp(-x/l)\exp(y/l)]$.

Next, we assume that the surface is isotropic in one dimension only, the y direction. We can integrate over $d\phi$ to obtain the form of $dp/d\theta$. We know that $d\Omega$ is

$$d\Omega = d\theta_s d\phi_s \sin\theta_s \cdot \tag{A3}$$

We have

$$dq = 2\pi df_y = \frac{2\pi}{\lambda} dk_y = \frac{2\pi}{\lambda}\sin\theta_s \cos\phi_s d\phi_s \cdot \tag{A4}$$

When Eq. (A4) is substituted into Eq. (A3), one has

$$d\Omega = \frac{d\theta \sin\theta_s dq}{\frac{2\pi}{\lambda}\sin\theta_s \cos\theta_s} = d\theta \times \frac{dq}{\frac{2\pi}{\lambda}\cos\phi_s}. \tag{A5}$$

With the assumptions of separability and one-dimensional isotropicity, $dq/d\theta$ can be obtained by integrating Eq. (A2) over all ranges of q instead of ϕ by using Eq. (A5).

Thus Eq. (A2) becomes

$$\frac{dP}{d\theta} = \frac{16\pi^2}{\lambda^4}[F_0]\frac{\sigma^2}{\frac{2\pi}{\lambda}\cos\phi_s}\int_{-\infty}^{\infty}\int_{-\infty}^{\infty}\int_{-\infty}^{\infty}\exp(-x/l)$$

$$\times \exp(-j2\pi x f_x)dx \exp(-y/l)\exp(-j2\pi x f_y)dy. \tag{A6}$$

But

$$\int_{-\infty}^{\infty}\exp(-x/l)\exp(-j2\pi x f_x)dx = \frac{2l}{1+(2\pi f_x l)^2}$$

$$= \frac{2l}{1+(pl)^2}, \tag{A7}$$

$$\int_{-\infty}^{\infty}\exp(y/l)\exp(-j2\pi y f_y)dy = \frac{2l}{1+(2\pi f_y l)^2}$$

$$= \frac{2l}{1+(ql)^2}. \tag{A8}$$

Equation (A6) becomes

$$\frac{dP}{d\theta} = \frac{16\pi^2}{\lambda^4}[F_0]\frac{\sigma^2}{\frac{2\pi}{\lambda}\cos\theta_s}\frac{2l}{1+(pl)^2}\int_{-\infty}^{\infty}\frac{2l}{1+(ql)^2}dq. \tag{A9}$$

However,

$$\int_{-\infty}^{\infty}\frac{l}{1+(ql)^2}dq = \int_{-\infty}^{\infty}\frac{dx}{1+x^2} = \pi \qquad (\text{let } ql = x). \tag{A10}$$

Equation (A9) reduces to

$$\frac{dP}{d\theta} = \frac{16\pi^2}{\lambda^4}[F_0]\frac{\sigma^2}{\frac{2\pi}{\lambda}\cos\phi_s}\times\frac{2l}{1+(pl)^2}2\pi$$

$$= \frac{16\pi^2}{\lambda^3}[F_0]\frac{1}{\cos\phi_s}\times\frac{2\sigma^2 l}{1+(pl)^2}$$

$$= \frac{16\pi^2}{\lambda^3}[F_0]\frac{2\sigma^2 l}{1+(pl)^2} \qquad (\cos\phi_s = 1 \text{ in the plane}). \tag{A11}$$

ACKNOWLEDGMENTS

We appreciate receiving the cooperation of and measurements made by Jean Bennett of the Naval Weapons Center, China Lake, California, the measurements made by James Wyant of the Optical Sciences Center, University of Arizona, Tucson, Arizona; and the comments of Eugene Church of the U.S. Army Armament Research and Development Command. The work was supported by the U.S. Air Force under contract F49620-80-C-0022.

Part of this research was presented at the Optical Society of America Annual Meeting, Tucson, Arizona, October 1982.

REFERENCES

1. H. Davies, "The reflection of electromagnetic waves from a rough surface," Proc. IEE 101, 209–214 (1954).
2. P. Beckmann and A. Spizzichino, *The Scattering of Electromagnetic Waves from Rough Surfaces* (Pergamon, New York, 1963).
3. For instance, J. E. Harvey, "Light-scattering characteristics of optical surfaces," Ph.D. Thesis (University of Arizona, Tucson, Ariz., 1976); P. J. Chandley and W. T. Welford, "A reformulation of some results of P. Beckmann for scattering from rough surfaces," Opt. Quantum Electron 7, 393–397 (1975).
4. S. Silver, *Microwave Antenna Theory and Design* (McGraw-Hill, New York, 1947), p. 161.
5. J. D. Jackson, *Classical Electrodynamics* (Wiley, New York, 1975).
6. E. L. Church, H. A. Jenkinson, and J. M. Zavada, "Measurement of the finish of diamond-turned metal surfaces by differential light scattering," Opt. Eng. 16, 360–374 (1977); J. E. Elson and J. M. Bennett, "Vector scattering theory," Opt. Eng. 18, 116–124 (1979); A. Marvin, F. Toigo, and V. Celli, "Light scattering from rough surfaces: general incidence angle and polarization," Phys. Rev. B 11, 2777–2782 (1975); A. A. Maradudin and D. L. Mills, "Scattering and absorption of electromagnetic radiation by a semi-infinite medium in the presence of surface roughness," Phys. Rev. *B 11, 1392–1415 (1975); D. E. Barrick and W. E. Peake*, "Scattering from surfaces with different roughness scales: analysis and interpretation," Tech. Rep. AD 662751 (Battelle Memorial Institute, 1967); A. Ishimaru, *Wave Propagation and Scattering in Random Media* (Academic, New York, 1978); E. Kroger and E. Kretschmann, "Scattering of light by slightly rough *surfaces or thin film including plasma resonance emission*," Ann. Phys. 237, 1–15 (1970).
7. Lord Rayleigh, *The Theory of Sound* (Dover, New York, 1945), Vol. 2.
8. D. Beaglehole and O. Hunderi, "Study of the interaction of light with rough metal surfaces, I. Experiment," Phys. Rev. B 2, 309–329 (1970); J. M. Elson and J. M. Bennett, "Relation between the angular dependence of scattering and the statistical properties of optical surfaces," J. Opt. Soc. Am. 69, 31–47 (1979); R. J. Noll and P. Glenn, "Mirror surface autocovariance functions and their associated visible scattering," Appl. Opt. 21, 1824–1838 (1982); J. Eastman and P. W. Baumeister, "The microstructure of polished optical surfaces," Opt. Commun. 12, 418–420 (1974); P. J. Chandley, "Determination of the autocorrelation function of height on a rough surface from coherent light scattering," Opt. Quantum Electron. 8, 329–333 (1976); J. M. Bennett, "Measurement of the rms roughness, autocovariance function and other statistical properties of optical surfaces using a FECO scanning interferometer," Appl. Opt. 15, 2705–2721 (1976)
9. *R. P. Young, "Metal-optics scatter measurement," Proc.* Soc. Photo-Opt. Instrum. Eng. 65, 57–62 (1975).
10. F. E. Nicodemus, "Reflectance nomenclature and directional reflectance and emissivity," Appl. Opt. 9, 1474–1475 (1970).
11. J. M. Bennett and J. H. Dancy, "Stylus profiling instrument for measuring statistical properties of smooth optical surfaces," Appl. Opt. 20, 1785–1802 (1981).
12. L. D. Brooks, "Microprocessor-based instrumentation for BRDF measurement from visible to FIR," Ph.D. Thesis (University of Arizona, Tucson, Ariz., 1982).
13. Measured by J. Wyant, Optical Sciences Center, University of Arizona, Tucson, Arizona. For reference see C. Koliopoulos, "Interferometric optical phase measurement techniques," Ph.D. Thesis (University of Arizona, Tucson, Ariz., 1981).

APPENDIX G

Use of BRDF data in determining surface roughness

Yaujen Wang and William L. Wolfe

Optical Sciences Center
University of Arizona, Tucson, Arizona 85721

Abstract

Vector theory has been used to obtain the power spectral density of the surface height distribution at several different wavelengths, conditions of polarization and geometries. The surface height was then determined both by integration and by curve fitting.

Introduction

One of the goals of the theory of surface scattering is to relate the scattered light to the surface properties. Determining both the correlation length ℓ and the rms roughness σ of a random surface might be considered the main problem of inverse scattering, although determining scaling laws and surface distribution functions are certainly of equal concern.

In previous publications we have shown rather good agreement between measurements at several wavelengths for different incidence angles and for different polarization and the vector version of electromagnetic theory.[1] Here we apply it to the determination of σ and ℓ. The BRDF written as f_r can be written[2]

$$f_r = F_\lambda F_o F_s \tag{1}$$

F_λ = wavelength factor

F_o = optical factor

F_s = surface factor

Appropriate expressions exist for each one of these factors. The optical factor is a complicated function of the angles of incidence and scattering, the form of which depends upon the polarization conditions. The wavelength factor is k^3 or k^4 depending upon whether the surface factor is assumed to be a one- or a two-dimensional power spectrum of the surface height distribution. The surface height power spectrum is then given by either of the two expressions

$$W_1(p) = \frac{2\sigma^2\ell}{1+p^2\ell^2}$$

$$W_2(p) = \frac{2\pi\sigma^2\ell^2}{(1+p^2\ell^2)^{3/2}} \tag{2}$$

The subscript indicates whether a one- or a two-dimensional form is assumed.

The value of σ can then be determined by several methods: a fit to the BRDF data, a fit to the inferred power spectrum, integration under the asymptotic approximation or a two-wavelength ratio technique. We discuss each technique in turn and then compare them.

BRDF curve fitting

We have taken our measured data in the past, assumed one of the two forms (actually W_1 worked better) of the surface power spectrum and used trial and error for determining σ and ℓ. This result should be expected from the form of the equations. We note that the determination depends upon the model for W.

Power spectrum curve fitting

The BRDF data can be divided by the appropriate surface factor to obtain the power spectrum of the surface. We did this for several different wavelengths, polarizations and incidence angles. The results showed that, at least for the sample we used, the power spectrum was one-dimensional. One can then find the values of σ and ℓ that give these power spectrum curves. Alternately one can integrate under the curve since the total integral of the power spectrum is $2\pi\sigma^2$. Numerical integration is tedious, so integration under the asymptotic approximation, described next, is appropriate. Note that with numerical integration or curve fitting to the power spectrum only the dimensionality of W is assumed and not its form.

Asymptotic methods

If the power spectrum can be properly represented by the one-dimensional model, as our sample can be, the curve can be represented asymptotically by two straight lines that intersect at (p_1,h). The integral, as shown in Appendix A is $2hp_1$ and this is equal to $2\pi\sigma^2$. We note that if the spectrum is two-dimensional the slope is -3 rather than -2 and the result is different but easily determined. This method depends upon both the dimensionality and the model.

Ratio technique for calculating ℓ

We now consider determining σ based on two measurements at the same value of $\beta-\beta_o$ but at different wavelengths. It can be seen immediately that the surface factors drop out. For either of the models we discussed σ also drops out. The expressions have only λ and $\beta-\beta_o$ in them. Either complicated algebraic manipulations or numerical techniques can then be used to obtain ℓ.

Results

Table 1 gives values of σ obtained by the BRDF fitting technique for a variety of angles, polarizations and wavelengths. The values obtained range from 11 to 42, a factor of almost 4. This is probably due to variations in individual measurements and inconsistency in the (tedious) curve fitting. Table 2 gives σ values obtained by three other different methods for the best estimate of the power spectrum using all three wavelengths. The agreement is better, but we should recognize the smoothing that results from using the three wavelengths. We also should note that no pp or uu data are included. Table 3 gives the correlation length obtained by the ratio technique. Table 4 gives values of the correlation length obtained by four different methods. Table 5 gives the rms surface height obtained by eight different ways. The last two are independent measurements made by Jim Wyant with a heterodyne interferometer and by Jean Bennett using a mechanical probe.

Table 1. RMS surface height found from curve fitting

	0.6328 μm	3.39 μm	10.6 μm
		<u>ss</u>	
-10°	26	41	42
+10°	27	26	28
-30°	41	40	39
+30°	40	42	41
-50°	28	48	40
+50°	26	25	27
		<u>pp</u>	
-10°	25	26	24
+10°	24	25	26
-30°	19	18	19
30°	18	19	17
-50°	14	13	14
50°	19	17	18
		<u>uu</u>	
-10°	15		
+10°			
-30°	16		
+30°			
-50°	11		
+50°			

Table 2. RMS surface height (Å)

Angle of incidence	Area integration of power spectrum (ss)	Curve-fitting on ss power spectrum	Asymptotic area integration of power spectrum
-10°	21.2	28.1	20
10°	16.7	22.5	18
-30°	23.9	33.5	25.2
30°	20.1	31.4	24.9
-50°	32.4	35.2	34.5
50°	32.0	43.1	35.7

Table 3. Correlation length from ratio technique

	ℓ (μm)
0.6328 ← 3.39 10°	9.09
3.39 ← 10.6 10°	10.08
0.6328 ↔ 10.6 10°	9.94
3.39 ↔ 10.6 -10°	8.55
0.6328 ↔ 10.6 -10°	10.74
0.6328 ↔ 3.39 -30°	8.91
Average	9.55

Table 4. Correlation length by four methods

	ℓ (μm)
Average of ℓ by ratio technique	9.55
Asymptotic method at long wavelength	12
Curve-fitting on ss BRDF	10
Curve-fitting on ss power spectrum	10

Table 5. Determination of rms surface height

	σ (Å)
area under ss power spectrum	24.4
asymptotic area under ss power spectrum	26.4
curve-fitting of ss BRDF data	32.3
curve-fitting of ss power spectrum	34.9
curve fitting of pp power spectrum	19
curve-fitting of uu power spectrum	14.1
Wyant	8
Bennett	7.5

Discussion

The autocorrelation length can be found a number of different ways. Some are dependent upon the entire model, some are independent of the surface factor (as long as it is independent of wavelength). All methods gave good agreement. They also agreed with an independent optical method, but they disagreed considerably with a mechanical method. The disagreement is still a matter of further study.

Several methods are available for obtaining the rms height. The method of BRDF curve fitting is tedious and completely model dependent. Power spectrum fitting requires no assumption about the surface factor. An assumption that the autocorrelation is exponentially decreasing is necessary for either fitting the curves or their asymptotes. The latter method is easy and seems as accurate as the data warrant. The ss data give σ values consistently higher than the other methods. This disagreement has been noted before and is still a matter of conjecture.

Table 6 provides a summary of the methods for determining the autocorrelation length, the source of data, the required assumptions and the apparent limitations. Table 7 is a similar presentation for the rms surface height.

Table 6. Methods for determining correlation length

	Data Source	Assumption	Limitations
BRDF curve fitting	BRDF data	Optical factor surface factor	Curve fitting error
Power spectrum curve-fitting	Power spectrum	Optical factor	Curve fitting error
Asymptotic in long wavelength	Power spectrum	Optical factor	Instrumental scattering
Ratio technique	BRDF data	Surface factor	Measurement error. Limited available data

Table 7. Methods for determining surface height

	Data source	Assumption	Limitations
BRDF curve fitting	BRDF data	Optical factor	Curve-fitting error
Power spectrum curve-fitting	Power spectrum	Optical factor	Curve-fitting error
Area integration of power spectrum	Power spectrum	Optical factor	Instrumental Scattering time consuming: tedious
Asymptotic area of power spectrum	Power spectrum	Optical factor Surface factor	Instrumental Scattering: fast, easy

Appendix A. Asymptotic integration

When the surface spectrum can be represented by two straight lines on a log-log plot, the integration is relatively simple. The area under the curve is given by

$$A = \int_0^{p_1} h \, dp + \int_{p_1}^{p_2} \frac{K}{p^m} \, dp \tag{3}$$

where K = constant
m = 2 or 3

This reduces to

$$A_1 = h p_1 + K \left(\frac{1}{p_1} - \frac{1}{p_2} \right) \tag{4}$$

$$A_2 = h p_1 + \frac{1}{2} K \left(\frac{1}{p_1^2} - \frac{1}{p_2^2} \right) \tag{5}$$

For most cases (all cases we have considered) p_2 is much greater than p_1 and the second term of the parenthesis may be ignored. At the intersection point

$$h = K/p_1^2 \text{ or } h = K/p_1^3 \qquad (6)$$

$$hp_1 = K/p_1 \quad hp_1 = K/p_1^2 \qquad (7)$$

Thus the two areas reduce to

$$A_1 = 2\ h\ p_1 \qquad (8)$$

$$A_2 = 1.5\ h\ p_1 \qquad (9)$$

These areas are equal to $2\pi\sigma^2$ so that

$$\sigma_1 = (h\ p_1/\pi)^{\frac{1}{2}} \qquad (10)$$

$$\sigma_2 = (3\ h\ p_1/4\pi)^{\frac{1}{2}} \qquad (11)$$

Appendix B. Ratio technique for calculating ℓ

We assume that BRDF measurements have been made at each of two wavelengths. Then

$$f_{r_1} = \frac{2}{\pi} k_1^2\ F_0\ 2\ \sigma^2\ell/[1+k_1^2(\beta-\beta_0)^2\ell^2] \qquad (12)$$

$$f_{r_2} = \frac{2}{\pi} k_2^3\ F_0\ 2\sigma^2\ell/[1+k_2^3(\beta-\beta_0)^2\ell^2] \qquad (13)$$

The ratio R is then found to be

$$R = \left(\frac{\lambda_2}{\lambda_1}\right)^3 \frac{[1 + k_2^2(\beta-\beta_0)^2\ell^2]}{[1 + k_1^2(\beta-\beta_0)^2\ell^2]} \qquad (14)$$

Let $R_\lambda = \lambda_2/\lambda_1$

Then

$$\frac{R}{R_\lambda^3}\left[1 + k_1^2(\beta-\beta_0)^2\right] = \left[1 + k_2^2(\beta-\beta_0)^2\right] \qquad (15)$$

$$\frac{R}{R_\lambda^3} - 1 = (2\pi)^2(\beta-\beta_0)^2\left[\left(\frac{1}{\lambda_2}\right)^2 - \left(\frac{1}{\lambda_1}\right)^2\right]\ell^2 \qquad (16)$$

$$\ell^2 = \frac{\left(\frac{R}{R_\lambda^3} - 1\right)(\lambda_1^2-\lambda_2^2)}{[2\pi(\beta-\beta_0)]^2(\lambda_1^2-\lambda_2^2)} \qquad (17)$$

Although further manipulation is possible, the solution for ℓ is apparent. It is given in terms of the two known wavelengths and the value of $\beta-\beta_0$. A similar result is obtainable for the two-dimensional case.

References

1. Wang, Y., and W. Wolfe, "Comparisons of surface scatter theory and experiment," to be submitted to Applied Optics.
2. Elson, J. M., and J. M. Bennett, J. Opt. Soc. Am. Vol. <u>69</u>, 31-47 (1978).